

1 **Inputs and processes affecting the distribution of** 2 **particulate iron in the North Atlantic along the GEOVIDE** 3 **(GEOTRACES GA01) section**

4
5
6 Arthur Gourain^{1,2}, H el ene Planquette¹, Marie Cheize^{1,3}, Nolwenn Lemaitre^{1,4}, Jan-Lukas
7 Menzel Barraqueta^{5,6}, Rachel Shelley^{1,7}, Pascale Lherminier⁸ and G eraldine Sarthou¹

8
9 1-UMR 6539/LEMAR/IUEM, CNRS, UBO, IRD, Ifremer, Technop ole Brest Iroise, Place Nicolas Copernic,
10 29280 Plouzan e, France

11 2- now at Ocean Sciences Department, School of Environmental Sciences, University of Liverpool, Liverpool,
12 L69 3GP, United Kingdom

13 3- now at Ifremer, Centre de Brest, G eosciences Marines, Laboratoire des Cycles G eochimiques (LCG), 29280
14 Plouzan e, France

15 4- now at Department of Earth Sciences, Institute of Geochemistry and Petrology, ETH-Z urich, Z urich,
16 Switzerland

17 5- GEOMAR, Helmholtz Centre for Ocean Research Kiel, Wischhofstra e 1-3, 24148 Kiel, Germany

18 6- now at Department of Earth Sciences, Stellenbosch University, Stellenbosch, 7600, South Africa

19 7- now at Earth, Ocean and Atmospheric Science, Florida State University, Tallahassee, Florida, 32310, USA

20 8- Ifremer, Univ. Brest, CNRS, IRD, Laboratoire d'Oc eanographie Physique et Spatiale (LOPS), IUEM, F-
21 29280, Plouzan e, France

22
23 *Correspondence to: helene.planquette@univ-brest.fr*

24 25 **Abstract**

26 The GEOVIDE cruise (May-June 2014, R/V *Pourquoi Pas?*) aimed to provide a better understanding on trace
27 metal biogeochemical cycles in the North Atlantic. As particles play a key role in the global biogeochemical cycle
28 of trace elements in the ocean, we discuss the distribution of particulate iron (PFe), in light of particulate
29 aluminium (PAI), manganese (PMn) and phosphorus (PP) distributions. Overall, 32 full vertical profiles were
30 collected for trace metal analyses, representing more than 500 samples. This resolution provides a solid basis for
31 assessing concentration distributions, elemental ratios, size-fractionation, or adsorptive scavenging processes in
32 key areas of the thermohaline circulation. Total particulate iron (PFe) concentrations ranged from as low as 9
33 pmol L⁻¹ in surface Labrador Sea waters to 304 nmol L⁻¹ near the Iberian margin, while median PFe concentrations
34 of 1.15 nmol L⁻¹ were measured over the sub-euphotic ocean interior.

35 Within the Iberian Abyssal Plain, ratio of PFe over PAI is identical to the continental crust ratio (0.21), indicating
36 the important influence of crustal particles in the water column. Overall, the lithogenic component explained more
37 than 87% of PFe variance along the section. Within the Irminger and Labrador basins, the formation of biogenic

38 particles led to an increase of the PFe/PAI ratio (up to 0.7 mol mol⁻¹) compared to the continental crust ratio (0.21
39 mol mol⁻¹). Margins provide high quantities of particulate trace elements (up to 10 nmol L⁻¹ of PFe) to the open
40 ocean, and in the case of the Iberian margin, horizontal advection of PFe was visible more than 250km away from
41 the margin. Additionally, several benthic nepheloid layers spreading over 200m above the seafloor were
42 encountered along the transect, especially in the Icelandic, Irminger and Labrador basins, delivering particles with
43 high PFe content, up to 89 nmol L⁻¹.

44

45 **1. Introduction**

46 Particles play a key role in the ocean where they drive the residence time of most elements (Jeandel and Oelkers,
47 2015), and strongly influence the global biogeochemistry of macro and micro-nutrients including iron (Milne et
48 al., 2017). In the surface ocean, biological activity produces biogenic suspended matter through planktonic
49 organisms, while atmospheric deposition (Baker et al., 2013; Jickells et al., 2005), riverine discharge (Aguilar-
50 Islas et al., 2013; Berger et al., 2008; Ussher et al., 2004) or ice-melting (Hawkings et al., 2014; Lannuzel et al.,
51 2011, 2014) bring mostly lithogenic derived particles to surface waters. These particulate inputs highly vary, both
52 spatially and seasonally, around the world's oceans. At depth, benthic and shelf sediment resuspension (e.g.
53 Aguilar-Islas et al., 2013; Cullen et al., 2009; Elrod et al., 2004; Fitzwater et al., 2000; Hwang et al., 2010; Lam
54 et al., 2015; Lam and Bishop, 2008; McCave and Hall, 2002), and hydrothermal activity (Elderfield and Schultz,
55 1996; Lam et al., 2012; Tagliabue et al., 2010, 2017; Trefry et al., 1985), provides important amounts of particles
56 to the water column. Moreover, authigenic particles can be produced *in-situ* by aggregation of colloids (Bergquist
57 et al., 2007) or oxidation processes (Bishop and Fleisher, 1987; Collier and Edmond, 1984). Thus, oceanic
58 particles result from a complex combination of these different sources and processes (Lam et al., 2015).

59 Particles represent the main part of the total iron pool in the upper water column (Radic et al., 2011), and strongly
60 interact with the dissolved pool (e.g. Ellwood et al., 2014). Indeed, dissolved iron can be scavenged onto particles
61 (Gerringa et al., 2015; Rijkenberg et al., 2014), incorporated into biogenic particles (Berger et al., 2008) or
62 produced by remineralisation of particles (Dehairs et al., 2008; Sarthou et al., 2008). Interestingly, the concept of
63 “reversible scavenging” (i.e. release at depth of dissolved iron previously scavenged onto particles) has been
64 advocated recently (Dutay et al., 2015; Jeandel and Oelkers, 2015; Labatut et al., 2014), while other studies reveal
65 distinct dissolution processes (e.g. Oelkers et al., 2012; Cheize et al., 2018). Slow dissolution of particulate iron
66 at margins has also been evoked as a continuous fertilizer of primary production and should be considered as a
67 source of dissolved iron (e.g. Jeandel et al., 2011; Jeandel and Oelkers, 2015; Lam and Bishop, 2008). Within or
68 below the mixed layer, the rates of regeneration processes can also impact the bioavailable pool of iron, among
69 other trace metals (e.g. Ellwood et al., 2014; Nuester et al., 2014). However, the rates of these processes are not
70 yet fully constrained. The study of particulate iron is thus essential to better constrain its marine biogeochemical
71 cycle. This subject received a growing interest over the last 10 years in particular (e.g. Bishop and Biscaye, 1982;
72 Collier and Edmond, 1984; Frew et al., 2006; Lam et al., 2012; Milne et al., 2017; Planquette et al., 2011, 2013;
73 Sherrell et al., 1998) and, to our knowledge, only two have been performed at an ocean-wide scale and published
74 so far: the GA03 GEOTRACES North Atlantic Zonal Transect (Lam et al., 2015; Ohnemus and Lam, 2015) and
75 the GP16 GEOTRACES Pacific Transect (Lam et al., 2017; Lee et al., 2017).

76 In this context, this paper presents the particulate iron distribution in the North Atlantic Ocean, along the
77 GEOTRACES GA01 section (GEOVIDE), and discusses the various sources and processes affecting its
78 distribution, using particulate aluminium, phosphorus or manganese.

79

80 **2. Methods**

81 *2.1. Study area*

82 Particulate samples were collected at 32 stations during the GEOVIDE (GEOTRACES GA01 section) cruise
83 between May and June 2014 aboard the R/V *Pourquoi Pas?* in the North Atlantic (Sarhou et al., 2018). The
84 sampling spanned several biogeochemical provinces (Figure 1) that first comprised the Iberian margin (IM,
85 Stations 2, 4 and 1), the Iberian Abyssal Plain (IAP, Stations 11 to 17), the Western European Basin (WEB, Station
86 19 to Station 29) and the Icelandic Basin (IcB, Stations 32 to 36). Then, samples were collected above the
87 Reykjanes Ridge (RR, Station 38), in the Irminger Basin (IrB, Stations 40 to 60), close to the Greenland shelf
88 (GS, Stations 53, 56 and 61), the Labrador Basin (LB, Stations 63 to 77) and finally close the Newfoundland shelf
89 (NS, Station 78) (Figure 1). The North Atlantic is characterized by a complex circulation (briefly described in
90 section 3.1 and in detail by Zunino et al. (2017) and García-Ibáñez et al. (2015) and is one of the most productive
91 regions of the global ocean (Martin et al., 1993; Sanders et al., 2014), with a complex phytoplankton community
92 structure composed of diverse taxa (Tonnard et al., in prep.).

93

94

95 *2.2. Sampling*

96 Samples were collected using the French GEOTRACES clean rosette, equipped with twenty-two 12L GO-FLO
97 bottles (two bottles were leaking and were never deployed during the cruise). GO-FLO bottles (General Oceanics)
98 were initially cleaned in the home laboratory (LEMAR) following the GEOTRACES procedures (Cutter and
99 Bruland, 2012). The rosette was deployed on a 14mm Kevlar cable with a dedicated, custom-designed clean
100 winch. Immediately after recovery, the GO-FLO bottles were individually covered at each end with plastic bags
101 to minimize contamination. They were then transferred into a clean container (class-100) for sampling. On each
102 cast, nutrient and/or salinity samples were taken to check potential leakage of the GO-FLO bottles.

103 Filters were cleaned following the GEOTRACES protocols (<http://www.geotraces.org/images/Cookbook.pdf>)
104 and kept in acid-cleaned 1 L LDPE bottles (Nalgene) filled with ultrapure water (Milli-Q, resistivity of 18.2 MΩ
105 cm) until use. All filters were 25 mm diameter in order to optimize signal over the filter blank except at the surface
106 depth where 47 mm diameter filters mounted on acid-cleaned polysulfone filter holders (Nalgene™) were used.
107 Prior to filtration, the GO-FLO bottles were shaken three times, as recommended in the GEOTRACES cookbook
108 to avoid settling of particles in the lower part of the bottle. GO-FLO bottles were pressurized to <8 psi with 0.2
109 μm filtered dinitrogen (N₂, Air Liquide). Seawater was then filtered directly through paired filters (Pall Gelman
110 Supor™ 0.45 μm polyetersulfone, and Millipore mixed ester cellulose MF 5 μm) mounted in Swinnex
111 polypropylene filter holders (Millipore), following Planquette and Sherrell (2012) inside the clean container.
112 Filtration was operated until the bottle was empty or until the filter clogged; volume filtered ranged from 2 liters
113 for surface samples to 11L within the water column. After filtration, filter holders were disconnected from the
114 GO-FLO bottles and a gentle vacuum was applied using a syringe in order to remove any residual water under a

115 laminar flow hood. Filters were then removed from the filter holders with plastic tweezers that were rinsed with
116 Milli-Q between samples. Most of the remaining seawater was ‘sipped’ by capillary action, when placing the non-
117 sampled side of the filter onto a clean 47 mm supor filter. Then, each filter pair was placed in an acid-cleaned
118 polystyrene PetriSlides (Millipore), double bagged, and finally stored at -20°C until analysis at LEMAR. Between
119 casts, filter holders were thoroughly rinsed with Milli-Q, placed in an acid bath (5% Trace metal grade HCl) for
120 24 hours, then rinsed with Milli-Q.

121 At each station, process blanks were collected as follows: 2L of a deep (1000 m) and a shallow (40 m) seawater
122 samples were first filtered through a 0.2 µm pore size capsule filter (Pall Gelman Acropak 200) mounted on the
123 outlet of the GO-FLO bottle before to pass through the particle sampling filter, which was attached directly to the
124 swinnex filter holder.

125

126 2.3. Analytical methods

127 Back in the home laboratory, sample handling was performed inside a clean room (Class 100). All solutions were
128 prepared using ultrapure water (Milli-Q) and all plasticware had been acid-cleaned before use. Frozen filters,
129 collected within the mixed layer depth or within nepheloid layers, were first cut in half using a ceramic blade: one
130 filter half was dedicated to total digestion (see below), while the other half was archived at -20°C for SEM analyses
131 or acid leaching of “labile” metals (Berger et al., 2008; to be published separately).

132 Filters were digested following the method described in Planquette and Sherrell (2012). Filters were placed on the
133 inner wall of acid-clean 15mL PFA vials (Savillex™), and 2 mL of a solution containing 2.9 mol L⁻¹ hydrofluoric
134 acid (HF, suprapur grade, Merck) and 8 mol L⁻¹ nitric acid (HNO₃, Ultrapur grade, Merck) was added to each vial.
135 Vials were then closed and refluxed at 130°C on a hot plate for 4 hours and filters removed. After cooling, the
136 digest solution was evaporated at 110°C until near dryness. Then, 400 µL of concentrated HNO₃ (Ultrapur grade,
137 Merck) was added, and the solution was re-evaporated at 110°C. Finally, the obtained residue was dissolved with
138 3mL of a 0.8 mol L⁻¹ HNO₃ (Ultrapure grade, Merck). This archive solution was transferred to an acid cleaned 15
139 mL polypropylene centrifuge tube (Corning®) and stored at 4°C until analyses.

140 All analyses were performed on a sector field inductively coupled plasma mass spectrometer (SF-ICP-MS
141 Element2, Thermo-Fisher Scientific). Samples were diluted by a factor of 7 on the day of analysis in acid-washed
142 13 mm (outer diameter) rounded bottom, polypropylene centrifuge tubes (VWR) with 0.8 mol L⁻¹ HNO₃ (Ultrapur
143 grade, Merck) spiked with 1µg L⁻¹ of Indium (¹¹⁵In) solution in order to monitor the instrument drift. Samples
144 were introduced with a PFA-ST nebulizer connected to a quartz cyclonic spray chamber (Elemental Scientific
145 Incorporated, Omaha, NE) via a modified SC-Fast introduction system consisting of an SC-2 autosampler, a six-
146 port valve and a vacuum-rinsing pump. The autosampler was contained under a HEPA filtered unit (Elemental
147 Scientific). Two 6-points, matrix-matched multi-element standard curves with concentrations bracketing the range
148 of the samples were run at the beginning, the middle and the end of each analytical run. Analytical replicates were
149 made every 10 samples, while accuracy was determined by performing digestions of the certified reference
150 material BCR-414 (plankton, Community Bureau of Reference, Commission of the European Communities),
151 PACS-3 and MESS-4 (marine sediments, National Research Council Canada), following the same protocol as for
152 samples. Recoveries were typically within 10% of the certified values (and within the error of the data, taken from
153 replicate measurements, Table 1). Once all data were normalized to an ¹¹⁵In internal standard and quantified using
154 an external standard curve, the dilution factor of the total digestion was accounted for. Obtained element

155 concentrations per filter (pmol/filter) were then corrected by the process blanks described above. Finally,
156 pmol/filter values were divided by the volume of water filtered through stacked filters.
157 Total concentrations (sum of small size fraction (0.45-5 µm) and large (>5 µm) size fraction) of particulate trace
158 elements are reported in Table S1.

159

160

2.4. Positive matrix factorisation

161 Positive Matrix Factorisation (PMF) was run to characterise the main factors influencing the particulate trace
162 elements variances along the GEOVIDE section. In addition to PFe, PAI, PMn, and PP, nine additional elements
163 were included in the PMF: Y, Ba, Pb, Th, Ti, V, Co, Cu and Zn. The analysis has been conducted on samples
164 where all the 13 elements previously cited were above the detection limits; after selection, 445 of the 549 existing
165 data points were used. Analyses were performed using the PMF software, EPA PMF 5.0, developed by the USA
166 Environmental Protection Agency (EPA). Models have been tested with several factors number (from 3 to 6),
167 after full error estimation of each model, we decide to use the configuration providing the lowest errors estimations
168 and in consequence the most reliable.

169 In consequence, models were set up with four factors and were run 100 times to observe the stability of the
170 obtained results. After displacement, error estimations and bootstraps error estimations, the model was recognised
171 as stable.

172

173

2.5. Derived and ancillary parameters

174 To investigate the proportion of lithogenic iron within the bulk particulate iron, we use the Upper Continental
175 Crust (UCC) Fe/Al molar ratio of Taylor and McLennan (1995), 0.21, to calculate the lithogenic components of
176 particles (%PFe_{litho}) following Eq. (1):

177

$$178 \quad \%PFe_{litho} = 100 * \left(\frac{PAI}{PFe} \right)_{sample} * \left(\frac{PFe}{PAI} \right)_{UCC \text{ ratio}} \quad (1)$$

179

180 Then the non-lithogenic PFe is obtained using Eq. (2):

181

$$182 \quad \%PFe_{non_litho} = 100 - \%PFe_{litho} \quad (2)$$

183

184 Note that while the %PFe_{litho} and %PFe_{non-litho} proxies are interesting tools to evaluate the importance of lithogenic
185 and non-lithogenic (either biogenic or authigenic), they have to be used carefully, as spatial and temporal variation
186 of the lithogenic component ratios may falsely influence the estimated fraction value.

187

188 In addition to PAI, PMn can be used as a tracer of inputs from shelf resuspension (Lam and Bishop, 2008). Indeed,
189 Mn is really sensitive to oxidation mediated by bacteria (Tebo et al., 1984; Tebo and Emerson, 1985) and forms
190 manganese oxides (MnO₂). These authigenic particles lead to an enrichment of Mn in particle compositions. In
191 order to track the influence of shelf resuspension, a percentage of sedimentary inputs “%bulk sediment inputs”
192 can be estimated using PMn/PAI ratio from GEOVIDE samples and the PMn/PAI UCC value (0.0034; Taylor and
193 McLennan, 1995) according to the following equation:

194
$$\% \text{bulk sediment PMn} = 100 * \left(\frac{\text{PAI}}{\text{PMn}} \right)_{\text{sample}} * \left(\frac{\text{PMn}}{\text{PAI}} \right)_{\text{UCC ratio}} \quad (3)$$

195 This proxy can be a good indicator of direct and recent sediment resuspension. We assume that particles newly
196 resuspended in water column will have the same PMn/PAI ratio than the UCC ratio leading to a “%bulk sediment
197 Mn” of 100%. This value will decrease by authigenic formation of Mn oxides. This proxy assumes homogeneity
198 of the sediment PMn/PAI ratio through the section which may not be completely the case at every station. In
199 consequence, this proxy is only a tool to identify new benthic resuspension at specific location and inter-
200 comparison between several locations is not possible. When a sample presents a “%bulk sediment Mn” greater
201 than 100%, we assign a value of 100% to simplify the following discussion. As the Mn cycle can also be affected
202 by biologic uptake (e.g. Peers and Price, 2004; Sunda and Huntsman, 1983), this proxy is only used at depths
203 where biologic activity is negligible (i.e. below 150m depth).

204 Potential temperature (θ°), salinity (S), and transmissometry data were retrieved from the CTD sensors (CTD
205 SBE911 equipped with a SBE43).

206

207

208 **3. Results**

209

3.1. Hydrography setting

210 Here, we briefly describe the hydrography encountered during the GEOVIDE section (Figure 2), as a thorough
211 description is available in García-Ibáñez et al. (2015). In the beginning of the section, the warm and salty
212 Mediterranean Water (MW, S=36.50, $\theta^\circ=11.7^\circ\text{C}$) was sampled between 600 and 1700 m in the Iberian Abyssal
213 Plain (IAP). MW resulted from the mixing between the Mediterranean Overflow Water plume coming from the
214 Mediterranean Sea and local waters. Surface water above the Iberian Shelf was characterised by low salinity
215 (S=34.95) at station 2 and 4 compared to surrounding water masses. Close to the floor of the Iberian Abyssal
216 Basin, the North East Atlantic Deep Water (NEADW, S=34.89, $\theta^\circ=2.0^\circ\text{C}$) spread northward. The North Atlantic
217 Central Water (NACW, S>35.60, $\theta^\circ>12.3^\circ\text{C}$) was the warmest water mass of the transect and was observed in
218 the subsurface layer of the Western European Basin and Iberian Abyssal Plain. An old Labrador Sea Water (LSW,
219 S=34.87, $\theta^\circ=3.0^\circ\text{C}$) flowed inside the Western European and Icelandic Basins, between 1000 and 2500m depth.
220 In the Icelandic Basin, below the old LSW, the Iceland-Scotland Overflow Water (ISOW, S=34.98, $\theta^\circ=2.6^\circ\text{C}$)
221 spread along the Reykjanes Ridge slope. This cold water, originating from the Arctic, led to the formation of
222 NEADW after mixing with surrounding waters. North Atlantic hydrography was impacted by the northward
223 flowing of the North Atlantic Current (NAC), which carried up warm and salty waters from the subtropical area.
224 By air-sea interactions and mixing with surrounding water, the NACW is cooled down and freshened in the
225 subpolar gyre and is transformed in Subpolar Mode Water (SPMW). The formation of SPMW inside the Icelandic
226 and Irminger Basins led to the formation of regional modal waters: the Iceland Subpolar Mode Water (IcSPMW,
227 S=35.2, $\theta^\circ=8.0^\circ\text{C}$) and the Irminger Subpolar Mode Water (IrSPMW, S=35.01, $\theta^\circ=5.0^\circ\text{C}$) respectively. IcSPMW
228 was a relatively warm water mass with potential temperature up to 7°C (García-Ibáñez et al., 2015). Another
229 branch of the NAC mixed with Labrador Current waters to form the relatively fresh SubArctic Intermediate Water
230 (SAIW, S=<34.8, $4.5^\circ\text{C}<\theta^\circ<6^\circ\text{C}$).

231 The Irminger Basin is a complex area with a multitude of water masses. In the middle of the basin, an old LSW,
232 formed one year before (Straneo et al., 2003), spread between 500 and 1200 m depth. Close to the bottom, the
233 Denmark Strait Overflow Water (DSOW, $S=34.91$) flowed across the basin. Greenland coastal waters were
234 characterised by low salinity values, down to $S=33$. The strong East Greenland Current (EGC) flowed southward
235 along the Greenland shelf in the Irminger Basin. When reaching the southern tip of Greenland, this current entered
236 the Labrador Basin along the west coast of Greenland and followed the outskirts of the basin until the
237 Newfoundland shelf. In the Labrador Basin, the deep convection of SPMW at 2000 m was involved in the
238 formation of the LSW ($S=34.9$, $\theta^{\circ}C=3.0^{\circ}C$) (García-Ibáñez et al., 2015; Yashayaev and Loder, 2009). Above the
239 Newfoundland Shelf, surface waters were affected by discharge from rivers and ice-melting and characterised by
240 extreme low salinity for open ocean waters, below 32 in the first 15 meters.

241 3.2. Section overview

242 Total particulate iron, aluminium, manganese and phosphorus concentrations spanned a large range of
243 concentrations from below detection to 304, 1544, 3.5 and 402 nmol L^{-1} respectively. The ranges of concentrations
244 are comparable to other studies recently published (Table 2).

245 PFe, PAI, and PMn were predominantly found (>90%) in particles larger than 5 μm , except in surface waters,
246 where 9 ± 8.6 % of PFe, 10.9 ± 15.4 % of PAI and 32.8 ± 16.6 % of PMn, 38.8 ± 8.6 % of PP were hosted by
247 smaller particles (0.45-5 μm). Data are shown in Figure 3.

248

249 3.3. Open Ocean stations: from the Iberian Abyssal Plain to the Labrador Basin

250 This concerns all stations from station 11 to 77, with the exception of stations 53, 56 and 61 that were sampled
251 close to the Greenland coast (Figure 1). Particulate iron concentration profiles showed identical patterns at all of
252 the open ocean stations encountered along the section. Median PFe were low at 0.25 nmol L^{-1} within the first 100
253 m and steadily increased with depth. However, at two stations, elevated concentrations were determined in the
254 upper 100m, up to 4.4 nmol L^{-1} at station 77 at 40 m and 7 nmol L^{-1} at station 63 between 70 and 100 m depth.
255 PFe concentrations gradually increased with depth, with a median PFe of 1.74 nmol L^{-1} below 1000m. Close to
256 the seafloor of some stations (26, 29, 32, 34, 49, 60, and 71), high concentrations of PFe were observed, up to 88
257 nmol L^{-1} (station 71 at 3736 m). These high PFe values were associated with low beam transmissometry value
258 inferior or equal to 97%.

259 Particulate aluminium (PAI) and manganese (PMn) profiles were similar to PFe profiles, with low concentrations
260 measured in the first 100 m (1.88 nmol L^{-1} and 55 pmol L^{-1} , respectively) and increased towards the seafloor.
261 Close to the seafloor, high concentrations were determined at the same stations cited above for PFe, with a
262 maximum of 264 nmol L^{-1} and 3.5 nmol L^{-1} for PAI and PMn respectively at station 71 (supplementary Table S1).
263 Highest particulate phosphorus (PP) concentrations were in the first 50m, with a median value of 66 nmol L^{-1} .
264 Deeper in the water column, below 200m, PP concentrations decreased to values below 10 nmol L^{-1} . Inter-basins
265 differences were observed within the surface samples, with median PP concentration being higher in the Irminger
266 Basin (127 nmol L^{-1}) than in the Iberian Abyssal Plain (28 nmol L^{-1}) (Figure 3).

267 Finally, above the Reykjanes Ridge, PP, PMn, PAI and PFe concentrations were in the same range than the
268 surrounding open ocean stations. However, close to the seafloor, high concentrations were measured, with PFe,
269 PAI, and PMn reaching 16.2 nmol L⁻¹, 28.8 nmol L⁻¹, and 0.51 nmol L⁻¹ at 1354 m, respectively (Figure 3 and
270 Table S1).

271

272 3.4. Margins and Shelves: Iberian Margin (stations 1 to 4), Greenland coast (stations 53, 56
273 and 61) and Newfoundland Shelf (station 78)

274

275 The Iberian margin was characterised by low beam transmissometry values at station 2 (88% at 140 m, Figure 4b)
276 suggesting significant particle concentrations. Particulate iron concentrations varied between 0.02 nmol L⁻¹ to 304
277 nmol L⁻¹. Within the first 50m, PFe concentrations decreased towards the shelf break where PFe dropped down
278 from 2.53 nmol L⁻¹ (station 2) to 0.8 nmol L⁻¹ (Station 1). At all three stations, PFe concentrations increased with
279 depth and reached a maximum close to the seafloor. As an example, 300 nmol L⁻¹ of PFe was measured at 138.5m
280 at station 2. Lithogenic tracers, such as PAI or PMn, presented similar profiles to PFe with concentrations ranging
281 between 0.11 and 1544 nmol L⁻¹, and from below detection limit to 2.51 nmol L⁻¹ respectively (Figure 3, Table
282 S1). Total particulate phosphorus (PP) concentrations were relatively low in the surface ranging from undetectable
283 values to 38 nmol L⁻¹; concentrations decreased with depth and were less than 0.7 nmol L⁻¹ below 1000 m depth.
284 In the vicinity of the Greenland shelf, PFe concentrations had a high median value of 10.8 nmol L⁻¹ and were
285 associated with high median PAI and PMn concentrations of 32.3 nmol L⁻¹ and 0.44 nmol L⁻¹, respectively.
286 Concentrations of PP were high at the surface with a value of 197 nmol L⁻¹ at 25 m of station 61. Then, PP
287 concentrations decreased strongly, less than 30 nmol L⁻¹, below 100 meters depth. Furthermore, beam
288 transmissometry values in surface waters at these three stations, were the lowest of the entire section, with values
289 below 85%.

290 Close to the Newfoundland margin, surface waters displayed a small load of particulate trace metals as PFe, PAI,
291 and PMn were below 0.8 nmol L⁻¹, 2 nmol L⁻¹, and 0.15 nmol L⁻¹ respectively. Then close to the bottom of station
292 78, at 371 m, beam transmissometry values dropped to 94% and were associated with extremely high
293 concentrations of PFe=168 nmol L⁻¹, PAI=559 nmol L⁻¹, and PMn=2 nmol L⁻¹. Total PP concentrations in the first
294 50 m ranged from 35 to 97 nmol L⁻¹. Below, PP remained relatively high with values up to 16 nmol L⁻¹ throughout
295 the water column. (Figure 3 and Table S1).

296

297 **4. Discussion**

298 Our goal in this work was to investigate mechanisms that drive the distribution of PFe in the North Atlantic, in
299 particular the different routes of supply and removal. Possible candidate sources of PFe include lateral advection
300 offshore from margins, atmospheric inputs, continental run-off, melting ice shelves and icebergs, resuspended
301 sediments, hydrothermal inputs and biological uptake. Removal processes include remineralization, dissolution
302 processes and sediment burial.

303 In the following sections, we examine each of these sources and processes, explore the evidence for their relative
304 importance, and use compositional data to estimate the particle types and host phases for iron and associated
305 elements.

306 4.1. Analysis of the principal factors controlling variance: near-ubiquitous influence of crustal
307 particles in the water column

308 The positive matrix factorisation analysis (Figure 5) has been realised on the entire dataset, in consequence, the
309 factors described below are highly influenced by the major variations of particulate element concentrations
310 (usually at the interface, i.e. margin, seafloor, surface layer). The first factor is characterised by lithogenic
311 elements, representing 86.8% of the variance of PFe, 75.8% of PAI and 90.5% of PTi. The second factor is
312 correlated with both Mn and Pb and explains no less than 76.5% and 77.0% of their respective variances. Ohnemus
313 and Lam (2015) observed this co-relation between manganese and lead particles and explained it by the co-
314 transport on Mn-oxides (Boyle et al., 2005). The formation of barite is causing the third factor constraining 87.7%
315 of the Ba variance in the studied regions. Biogenic barite accumulation within the mesopelagic layer is related to
316 bacterial activity and remineralisation of biogenic material (Lemaitre et al., 2018a). A biogenic component is the
317 fourth factor and explained most of particulate phosphorus variance, 83.7%. The micronutrient trace metals,
318 copper, cobalt and zinc, had more than a quarter of their variances influenced by this factor. Note that the biogenic
319 contribution to particulate iron and other trace elements will be discussed in another paper (Planquette et al., in
320 prep).

321 These results indicate that along the GA01 section, PFe distributions were predominantly controlled by lithogenic
322 material and to a smaller extent by remineralisation processes (as seen by a Factor 3 contribution of 4.1%). This
323 does not rule out some biogenic influence on PFe distribution, especially in surface, but this contribution is veiled
324 by the high lithogenic contribution.

325 To further investigate the influence of crustal material on the distribution of PFe, it is instructive to examine the
326 distribution of the molar ratio of PFe/PAI, and the resulting %PFe_{litho} (see section 2.6 for definition of this
327 parameter) along the section (Figure 6). Overall, the estimated lithogenic contribution to PFe varies from 25%
328 (station 60, 950 m) to 100% at stations located within the Western European Basin. Note that 100% of estimated
329 lithogenic PFe does not necessary mean that biogenic particles are absent; they may just be masked by the
330 important load of lithogenic particles. Important inter-basins variations are observed along the section (Figure 6).
331 The IAP and WEB basins are linked with high median value of the proxy %PFe_{litho}, 90%, which is also reflected
332 in the MW and NEADW PFe/PAI ratio, that displays a value close to the crustal one (Figure 7). This could be
333 linked to a lateral advection of iron rich lithogenic particles sourced from the Iberian margin and to atmospheric
334 particles (Shelley et al., 2017). This point is discussed with more detail in section 4.2.4. Then, between stations
335 26 and 29, the %PFe_{litho} proxy values dramatically decreased, and reached values under 55% in the Iceland,
336 Irminger and the Labrador basins. This feature is likely associated to the presence of the Sub-Arctic Front, located
337 between 49.5 and 51°N latitude and 23.5 and 22°W longitude (Zunino et al., 2017). Indeed, this front which
338 separates cold and fresh water of subpolar origin from warm and salty water of subtropical origin was clearly
339 identifiable by the steep gradient of the isohalines between station 26 and 29; salinity dropping from 35.34 to
340 35.01 (Figure 2). North of the Sub-Arctic Front, LSW and ISOW display high PFe/PAI ratios, ranging from 0.36
341 to 0.44 mol mol⁻¹. These high ratios, compared to the crustal one, could be associated to higher content of PFe
342 from biogenic origin, especially in the case of the LSW.

343

344 4.2. Tracking the different inputs of particulate iron

345

4.2.1. Inputs at margins: Iberian, Greenland and Newfoundland

346 Inputs from continental shelves and margins have been demonstrated to support high productivity in shallow
347 coastal areas. Inputs of iron from continental margin sediments supporting the high productivity found in shallow
348 coastal regions have been demonstrated in the past (e.g. Cullen et al. (2009), Elrod et al. (2004), Jeandel et al.
349 (2011), Ussher et al. (2007)) and sometimes, were shown to be advected at great distances from the coast (e.g.
350 Lam and Bishop, 2008). In the following section, we will investigate these possible candidate sources in proximity
351 of the different margins encountered.

352

353 *The Iberian margin*

354 The Iberian margin was an important source of lithogenic-derived iron-rich particles in the Atlantic Ocean during
355 GEOVIDE; shelf resuspension impact was perceptible until 280 km away from the margin (Station 11) in the
356 Iberian Abyssal Plain (Figure 8).

357 On the shelf, at station 2 high sediment resuspension was observable by low beam transmissometry value (87.6%)
358 at the immediate vicinity of the seafloor (153m). This sediment resuspension led to an extensive input of lithogenic
359 particles within the water column associated with high concentrations of PFe (304 nmol L⁻¹), PAI (1500 nmol L⁻¹)
360 and PMn (2.5 nmol L⁻¹) (Figure 3, Table S1). Moreover, 100% of PFe was estimated to have a lithogenic origin
361 (Figure 8) while 100% of the PMn was estimated to be the result of a recent sediment resuspension according to
362 the %Fe_{litho} and “%bulk sediment Mn” proxies (Figure 8), confirming the resuspended particle input. Besides,
363 ADCP data acquired during GEOVIDE (Zunino et al., 2017) and several studies have reported an intense current
364 spreading northward coming from Strait of Gibraltar and Mediterranean Sea, leading to a strong resuspension of
365 benthic sediments above the Iberian Shelf, e.g. Biscaye and Eittrreim (1977), Eittrreim et al. (1976), McCave and
366 Hall (2002), Spinrad et al. (1983).

367 At distance from the shelf, within the Iberian Abyssal Plain, an important lateral advection of PFe from the margin
368 was observable (Figure 8). These lateral inputs occurred at two depth ranges: between 400 and 1000 m as seen at
369 stations 4 and 1, with PFe concentrations reaching 4 nmol L⁻¹, and between 2500 m and the bottom (3575 m) of
370 station 1, with PFe concentrations reaching 3.5 nmol L⁻¹. While 100% of PFe had a lithogenic signature, the
371 sedimentary source input estimation decreased, between 40% and 90% of the PMn (Figure 8). Transport of
372 lithogenic particles was observable until station 11 (12.2°W) at 2500 m where PFe concentration was 7.74 nmol
373 L⁻¹ and 60% of PMn had a sedimentary origin (Figure 4). Noteworthy, no particular increase in PFe, PMn or PAI
374 was seen between 500 and 2000 m depth, where the MOW spreads, which is consistent with that was observed
375 DFe concentrations (Tonnard et al., this issue); yet in contrast with the dissolved aluminium values (Menzel-
376 Barraqueta et al, 2018, this issue) which were high in the MOW and with the study of Ohnemus and Lam (2015)
377 that reported a maximum PFe concentration at 695 m depth associated with the particle-rich Mediterranean
378 Overflow Water (Eittrreim et al., 1976) in the IAP. However, their station was located further south of our station
379 1. The shallower inputs observed at stations 1 and 4 could therefore be attributed to sediment resuspension from
380 the Iberian margin and nepheloid layer at depth for station 1.

381 Surface coastal waters of the Iberian Shelf are impacted by the runoff for the Tagus River, which is characterised
382 by high suspended matter discharges, ranging between 0.4 to 1 × 10⁶ tons yr⁻¹, and with a high anthropogenic
383 signature (Jouanneau et al., 1998). During the GEOVIDE section, the freshwater input was observable at stations

384 1, 2 and 4 in the first 20 m; salinity was below 35.2 while surrounding waters masses had salinity up to 35.7.
385 Within the freshwater plume, particulate concentrations were high at station 2 with PFe of 1.83 nmol L⁻¹. Further
386 away from the coast, the particulate concentrations remained low at 20m depth, with PFe, PAI, and PMn
387 concentrations of 0.77 nmol L⁻¹, 3.5 nmol L⁻¹, and 0.04 nmol L⁻¹, respectively at station 1. The low expansion of
388 the Tagus plume is likely due to the rapid settling of suspended matter. Indeed, our coastal station 2 was already
389 located at around 50 km of the Iberian coast and according to Jouanneau et al. (1998), the surface particle load
390 can be observable at a maximum 30km of the Tagus estuary. Overall, the Iberian margin appears to be an important
391 source of lithogenic-derived iron rich particles in the Atlantic Ocean.

392

393 *South Greenland*

394 Along GEOVIDE, Greenland shelves were a source of particulate-rich meteoric water leading to a transfer of DFe
395 to PFe by an enhanced biological activity. Indeed, both East and West Greenland shelves (stations 53 and 61) had
396 high concentration of particles (beam transmissometry of 83%) and particulate trace elements, reaching 22.1 nmol
397 L⁻¹ and 18.7 nmol L⁻¹ of PFe, respectively (station 53 at 100m and station 61 at 136 m). Several studies already
398 demonstrated the importance of icebergs and sea ice melting as sources of dissolved and particulate iron (e.g. van
399 der Merwe et al., 2011a, 2011b; Planquette et al., 2011; Raiswell et al., 2008). The Greenland shelf is highly
400 affected by external fresh water inputs such as sea-ice-melting or riverine runoff (Fragoso et al., 2016), that are
401 important sources of iron to the Greenland Shelf (Bhatia et al., 2013; Hawkings et al., 2014; Statham et al., 2008).
402 During the cruise, the relative freshwater observed (S<33 psu) within the first 25 meters of stations 53 and 61
403 were associated with high PFe (19 nmol L⁻¹), PAI (61 nmol L⁻¹), PMn (0.6 nmol L⁻¹) and a low beam
404 transmissometry (≤ 85%) (Figure 4 and Table S1). Particles associated were enriched in iron compared to
405 aluminium, as PFe/PAI ratio was 0.3 within the meteoric water plume. High biological production, in agreement
406 with PP concentrations reaching 197 nmol L⁻¹ induced by the supply of bioavailable dissolved iron from meteoric
407 water (Raiswell et al., 2008; Statham et al., 2008; Tonnard et al., submitted, this issue), led to a transfer of DFe
408 to the particulate phase. This is in line with the fact that around 30% PFe had a non-lithogenic origin. In addition,
409 only 40% PMn originated from resuspended sediments. Interestingly, these two proxies remained constant from
410 the seafloor to the surface (Station 49, Figure 8), with around 25% of the PMn of sedimentary origin, which could
411 be due to an important mixing happening on the shelf. The lithogenic PFe could result from the release of PFe
412 from Greenland bedrock captured during the ice sheet formation on land.

413 The spatial extent of the off-shelf lateral transport of particles was not important on the east Greenland coast.
414 Indeed, no visible increase of particulate trace metal concentrations was visible at the first station off-shelf, station
415 60 (Figure 8), except at 1000 m depth, where a strong increase (up to 90%) of sedimentary PMn was seen. This
416 is probably due to the East Greenland Coastal Current (EGCC) that was located at station 53 constrained these
417 inputs while stations 56 and 60 were under the influence of another strong current, the East Greenland-Irminger
418 current (EGIC) (Zunino et al., 2017). To the west of the Greenland margin, lateral transport of particles was
419 slightly more important. Noticeable concentrations of particulate lithogenic elements were observable until station
420 64 located 125 km away from shoreline. These particles had decreasing PFe lithogenic contribution (50%) with a
421 similar (25%) sedimentary PMn content than closer to the margin. The increasing nature of non-lithogenic PFe is
422 linked to the bloom in surface (associated with a PFe/PAI ratio of 0.30 mol mol⁻¹, a PP of 197 nmol L⁻¹ at station
423 61 and a Chl-a concentration of 6.21 mg m⁻³), with the biogenic PFe settling down along the transport of particles.

424 Therefore, particles newly resuspended from Greenland sediments are an important source, representing around
425 one third of the pMn pool, combined with surface inputs such as riverine runoff and/or ice-melting that are
426 delivering particles on the shelf and biological production. Unlike the Iberian shelf, Greenland margin was not an
427 important provider of particulate metals inside the Irminger and Labrador Basin, due to the circulation that
428 constrained the extent of the margin plume.

429

430

431

432 *The Newfoundland Shelf*

433 Previous studies already described the influence of fresh water on the Newfoundland shelf from the Hudson Strait
434 and/or Canadian Arctic Archipelago (Fragoso et al., 2016; Yashayaev, 2007). Yashayaev (2007) also monitored
435 strong resuspension of sediments associated with the spreading of Labrador Current along the West Labrador
436 margin.

437 Close to the Newfoundland coastline, at station 78, high fresh water discharge (≤ 32 psu) was observed in surface
438 (Benetti et al., 2017). Interestingly, these freshwater signatures were not associated with elevated particulate trace
439 metal concentrations. Distance of meteoric water sources implied a long travel time for the water to spread through
440 the Labrador Basin to our sampling stations. Along the journey, particles present originally may have been
441 removed from water column by gravitational settling.

442 The proportion of lithogenic PFe was relatively high and constant in the entire water column, with a median value
443 of 70%. At station 78, 100% of the PMn had a sedimentary origin close to the seafloor (371 m). The spreading of
444 the recent sediment resuspension was observable until 140 m depth where the contribution of sedimentary Mn
445 was still 51% (Figure 8, Table S2). This could correspond to an intense nepheloid layer as previously reported by
446 Biscaye and Eitrem (1977) (see also section 3.3.2). The high PFe concentration (184 nmol L^{-1} , station 78, 371
447 m) associated with a high percentage of sedimentary PMn (95%) observed at the bottom of this station, was
448 therefore the result of an important resuspension of shelf sediments. This was confirmed with low transmissometry
449 values of 95%.

450 The important phytoplanktonic community present (maximum Chl-a= 4.91 mg m^{-3} , Tonnard et al., in prep), is
451 linked to low PFe of 0.79 nmol L^{-1} at 10 m, but, with a high PFe/PAI ratio, up to 0.4, and PP concentration of 97
452 nmol L^{-1} , confirming the biologic influence. Either the biogenic particles settled quickly, and/or they were quickly
453 remineralized. Concerning this latter process, intense remineralization at station 77 ($7 \text{ mmol C m}^{-2} \text{ d}^{-1}$ compared
454 to $4 \text{ mmol C m}^{-2} \text{ d}^{-1}$ in the Western European Basin) has been reported by Lemaitre et al. (2018a and 2018b),
455 which could explain the low PFe values throughout the water column.

456

457

458 Along the GEOVIDE section, continental shelves provided an important load of particles within the surrounding
459 water column. The three margins sampled during GEOVIDE behaved differently; the Iberian margin discharged
460 high quantities of lithogenic particles far away from the coast while the Greenland and Newfoundland margins
461 did not reveal important PFe concentrations. Spreading of particles is tightly linked to hydrodynamic conditions,
462 which in the case of the Greenland margin, prevented long distance seeding of PFe. Moreover, each margin
463 showed a specific PFe/PAI ratio (Figure 9) indicating different composition of the resuspended particles.

464 Resuspended particles represent the composition of sediment at the margin if redox transformation of iron and
465 aluminium are considered negligible under these circumstances. Differences between margins were due to the
466 presence of non-crustal particles, either biogenic or authigenic. Biological production in surface waters and
467 authigenic formation of iron hydroxide produce particles with a higher PFe/PAI content and their export through
468 the water column to the sediment increased the PFe/PAI ratio at depth. Regions where biological production is
469 intense such as in the vicinity of Newfoundland presented higher PFe/PAI ratios of resuspended benthic particles.

470

471

4.2.2 Benthic resuspended sediments

472 Along the GEOVIDE section, Benthic nepheloid layers (BNLs) are providing high concentrations of particulate
473 trace element in the deep open ocean, contributing highly to the total trace elements budget as iron. Along the
474 GA01 section, BNLs were observable in each province with different strengths (Figures 3 and 10).

475

476 In BNLs located within the WEB, PFe concentrations reached up to 10 nmol L⁻¹ (stations 26 and 29, Table S1).
477 These concentrations were smaller than PFe concentrations encountered in BNL from the Icelandic (stations 32
478 and 34), Irminger (stations 42 and 44) and Labrador Basins (stations 68, 69 and 71), where benthic resuspension
479 led to PFe concentrations higher than 40 nmol L⁻¹, even reaching 89 nmol L⁻¹ at the bottom of station 71 (3736
480 m). Moreover, in the Irminger and Labrador Basins, PFe/PAI molar ratios within BNLs were higher than the ones
481 measured within the WEB at station 26 and 29. In the Irminger Basin, PFe/PAI reached 0.4 mol mol⁻¹ (Figure 10),
482 which could reveal a mixture of lithogenic and biogenic matter previously exported. This feature was also
483 observed in the Labrador Basin, with PFe/PAI ratio ranging between 0.34 and 0.44 mol mol⁻¹. In contrast, BNLs
484 sampled in the WEB have clearly a lithogenic imprint, with PFe/PAI molar ratios close to the crustal one.
485 Resuspended sediments with a non-crustal contribution seem to hold a higher PFe content than sediments with a
486 lithogenic characteristic. Nevertheless, interestingly all BNLs present during GEOVIDE were spreading
487 identically, with impacts observable up to 200 meters above the oceanic seafloor (Figure 10), as reflected in beam
488 transmissometry values, and PFe concentrations, that returned to a background level at 200 m above the seafloor.
489 The presence of these BNLs has also been reported by Le Roy et al. (submitted, this issue) using radium-226
490 activity. Important differences of PFe intensities could also be due to different hydrographic components and
491 topographic characteristics. BNLs are occurring due to strong hydrographic stresses (i.e. boundary currents,
492 benthic storms and deep eddies) interacting with the ocean floor (Biscaye and Eittrheim, 1977; Eittrheim et al., 1976;
493 Gardner et al., 2017, 2018). They are by definition highly variable geographically and temporally, but no physical
494 data could allow us to investigate further this hypothesis.

495

496

497

4.2.3. Reykjanes Ridge inputs

498 Above the ridge, high PFe concentrations were measured, reaching 16 nmol L⁻¹ just above the seafloor, while
499 increased DFe concentrations were reported to the East of the ridge (Tonnard et al., this issue). The exact sources
500 of iron-rich particles cannot be well constrained, as they could come from active hydrothermal vents or
501 resuspension of particulate matter from new crustal matter produced at the ridge. According to the oceanic
502 circulation (Zunino et al., 2017; Garcia-Ibanez et al., 2017), hydrothermal particles could have been seen in the

503 ISOW within the Icelandic Basin. Nevertheless, at the vicinity of the ridge, scanning electron microscope (SEM)
504 analyses of our samples did reveal a number of biological debris and clays but not the presence of iron
505 (oxy-)hydroxide particles (supplementary figure S1), which are known to be highly produced close to
506 hydrothermal vents (Elderfield and Schultz, 1996). Their absence could thus indicate an absence of vents.
507 However, other proxies, such as helium-3, are necessary to claim with more accuracy the presence or absence of
508 an hydrothermal source close to station 38.

509

510 4.2.4. Atmospheric inputs

511 Atmospheric deposition is an important input of trace elements in surface of the open ocean (e.g. (Jickells et al.,
512 2005). Atmospheric inputs, both wet and dry, were reported to be low during the GEOVIDE cruise (Menzel-
513 Barraqueta et al., 2018, this issue; Shelley et al., 2017; 2018). In fact, oceanic particles measurements in surface
514 waters along the section did not reveal high PFe or PAI concentrations. One pattern is interesting to note: the
515 surface waters of the Iberian Abyssal Plain and Western European Basin, between stations 11 and 23 presented a
516 characteristic feature with really low PFe/PAI elemental ratios, of 0.11, smaller than the UCC ratio of 0.21 (Figure
517 6). Such low ratios have been reported in the same region by Barrett et al. (2012). One possible explanation is
518 given by Buck et al. (2010) who described Fe-depleted aerosols in this area of the North Atlantic with PFe/PAI
519 ratio below UCC ratio. However, Shelley et al. (2017) found a higher PFe/PAI ratio around 0.25 in this area (their
520 sample geoa5-6). This result, highlights some of the difficulties that link atmospheric inputs to water column data
521 (Baker et al., 2016), and implies a probable fractionation after aerosol deposition. In addition, there is high spatial
522 and temporal variability of atmospheric deposition (Mahowald et al., 2005) and a certain degree of uncertainty
523 about the dissolution processes of atmospherically-transported particles (Bonnet and Guieu, 2004).

524

525

526 5. Conclusions

527

528 The investigation of the PFe compositions of suspended particulate matter along the GEOVIDE section in the
529 North Atlantic reflects the pervasive influence of crustal particles, augmented by sedimentary inputs at margins,
530 and within benthic nepheloid layers at depths. In consequence, variance of particulate iron along the section is
531 mainly explained by lithogenic factors.

532 Resuspension of sedimentary particles from continental shelves are responsible of high particulate iron
533 concentration within the surrounding water column, and could be observed at long distances, in the case of the
534 Iberian margin. Our results also demonstrate the impact of arctic meteoric water on the Greenland shelf while in
535 surface, the enhancement of productivity by new bioavailable iron is leading to a transfer of dissolved iron to the
536 particulate phase. Above the Reykjanes Ridge, resuspension of particles were responsible of the PFe enrichment
537 of the Iceland Scottish Overflow Water. Our dataset allowed the investigation of scavenging processes that were
538 sometimes visible at depths greater than 1000m, these effects being the most pronounced within the WEB.

539 Overall, particulate iron distribution in the North Atlantic is strongly affected by sources at its boundaries. This
540 work, within the frame of the GEOTRACES program, will allow a better understanding of the cycle of particulate
541 iron, when combined to other datasets in a modelling exercise for example.

542

543

544

545 **Acknowledgments**

546 We are greatly indebted to the captain and crew of the N/O Pourquoi Pas? for their help during the GEOVIDE
547 mission and clean rosette deployment. We would like to give special thanks to Fabien Pérault and Emmanuel de
548 Saint Léger for their technical expertise, to Catherine Schmechtig for the GEOVIDE database management and
549 Greg Cutter for his guidance in setting up the new French clean sampling system. We also would like to thanks
550 Reiner Schlitzer for the Ocean Data View software (ODV).

551 This work was supported by the French National Research Agency (ANR-13-BS06-0014, ANR-12-PDOC-0025-
552 01), the French National Centre for Scientific Research (CNRS-LEFE-CYBER), the LabexMER (ANR-10-
553 LABX-19), and Ifremer. It was supported for the logistic by DT-INSU and GENAVIR.

554

555 **References**

556 Aguilar-Islas, A. M., Rember, R., Nishino, S., Kikuchi, T. and Itoh, M.: Partitioning and lateral transport of iron
557 to the Canada Basin, *Polar Sci.*, 7(2), 82–99, doi:10.1016/j.polar.2012.11.001, 2013.

558 Baker, A. R., Adams, C., Bell, T. G., Jickells, T. D. and Ganzeveld, L.: Estimation of atmospheric nutrient inputs
559 to the Atlantic Ocean from 50°N to 50°S based on large-scale field sampling: Iron and other dust-associated
560 elements, *Global Biogeochem. Cycles*, 27(3), 755–767, doi:10.1002/gbc.20062, 2013.

561 Baker, A. R., Landing, W. M., Bucciarelli, E., Cheize, M., Fietz, S., Hayes, C. T., Kadko, D., Morton, P. L.,
562 Rogan, N., Sarthou, G., Shelley, R. U., Shi, Z., Shiller, A. and van Hulten, M. M. P.: Trace element and isotope
563 deposition across the air–sea interface: progress and research needs, *Philos. Trans. R. Soc. A Math. Phys. Eng.*
564 *Sci.*, 374(2081), 20160190, doi:10.1098/rsta.2016.0190, 2016.

565 Barrett, P. M., Resing, J. A., Buck, N. J., Buck, C. S., Landing, W. M. and Measures, C. I.: The trace element
566 composition of suspended particulate matter in the upper 1000m of the eastern North Atlantic Ocean: A16N, *Mar.*
567 *Chem.*, 142–144, 41–53, doi:10.1016/j.marchem.2012.07.006, 2012.

568 Benetti, M., Reverdin, G., Lique, C., Yashayaev, I., Holliday, N. P., Tynan, E., Torres-Valdes, S., Lherminier, P.,
569 Tréguer, P., and Sarthou, G.: Composition of freshwater in the spring of 2014 on the southern Labrador shelf and
570 slope, *Journal of Geophysical Research: Oceans*, 122, 1102–1121, 10.1002/2016jc012244, 2017.

571 Berger, C. J. M., Lippiatt, S. M., Lawrence, M. G. and Bruland, K. W.: Application of a chemical leach technique
572 for estimating labile particulate aluminum, iron, and manganese in the Columbia River plume and coastal waters
573 off Oregon and Washington, *J. Geophys. Res.*, 113, C00B01, doi:10.1029/2007JC004703, 2008.

574 Bergquist, B. A., Wu, J. and Boyle, E. A.: Variability in oceanic dissolved iron is dominated by the colloidal
575 fraction, *Geochim. Cosmochim. Acta*, 71(12), 2960–2974, doi:10.1016/j.gca.2007.03.013, 2007.

576 Bhatia, M. P., Kujawinski, E. B., Das, S. B., Breier, C. F., Henderson, P. B. and Charette, M. A.: Greenland
577 meltwater as a significant and potentially bioavailable source of iron to the ocean, *Nat. Geosci.*, 6(4), 274–278,
578 doi:10.1038/ngeo1746, 2013.

579 Biscaye, P. E. and Eitrem, S. L.: Suspended Particulate Loads and Transports in the Nepheloid Layer of the
580 Abyssal Atlantic Ocean, *Dev. Sedimentol.*, 23(C), 155–172, doi:10.1016/S0070-4571(08)70556-9, 1977.

581 Bishop, J. K. B. and Biscaye, P. E.: Chemical characterization of individual particles from the nepheloid layer in
582 the Atlantic Ocean, *Earth Planet. Sci. Lett.*, 58(2), 265–275, doi:10.1016/0012-821X(82)90199-6, 1982.

583 Bishop, J. K. B. and Fleisher, M. Q.: Particulate manganese dynamics in Gulf Stream warm-core rings and
584 surrounding waters of the N.W. Atlantic, *Geochim. Cosmochim. Acta*, 51(10), 2807–2825, doi:10.1016/0016-
585 7037(87)90160-8, 1987.

586 Bonnet, S. and Guieu C.: Dissolution of atmospheric iron in seawater, *Geophys. Res. Lett.*, 31(3), L03303,
587 doi:10.1029/2003GL018423, 2004.

588 Boyle, E. A., Bergquist, B. A., Kayser, R. A. and Mahowald, N.: Iron, manganese, and lead at Hawaii Ocean
589 Time-series station ALOHA: Temporal variability and an intermediate water hydrothermal plume, *Geochim.*
590 *Cosmochim. Acta*, 69(4), 933–952, doi:10.1016/j.gca.2004.07.034, 2005.

591 Buck, C. S., Landing, W. M., Resing, J. A. and Measures, C. I.: The solubility and deposition of aerosol Fe and
592 other trace elements in the North Atlantic Ocean: Observations from the A16N CLIVAR/CO2 repeat hydrography
593 section, *Mar. Chem.*, 120(1–4), 57–70, doi:10.1016/j.marchem.2008.08.003, 2010.

594 Cheize, M., Planquette, H. F., Fitzsimmons, J. N., Pelleter, E., Sherrell, R. M., Lambert, C., Bucciarelli, E.,
595 Sarthou, G., Le Goff, M., Liorzou, C., Chéron, S., Viollier, E., and Gayet, N.: Contribution of resuspended
596 sedimentary particles to dissolved iron and manganese in the ocean: An experimental study, *Chemical Geology*.
597 doi: 10.1016/j.chemgeo.2018.10.003, 2018.

598 Collier, R. and Edmond, J.: The trace element geochemistry of marine biogenic particulate matter, *Prog.*
599 *Oceanogr.*, 13(2), 113–199, doi:10.1016/0079-6611(84)90008-9, 1984.

600 Cullen, J. T., Chong, M. and Ianson, D.: British columbia continental shelf as a source of dissolved iron to the
601 subarctic northeast Pacific Ocean, *Global Biogeochem. Cycles*, 23(4), 1–12, doi:10.1029/2008GB003326, 2009.

602 Cutter, G. A. and Bruland, K. W.: Rapid and noncontaminating sampling system for trace elements in global
603 ocean surveys, *Limnol. Oceanogr. Methods*, 10(JUNE), 425–436, doi:10.4319/lom.2012.10.425, 2012.

604 Dammshäuser, A., Wagener, T., Garbe-Schönberg, D. and Croot, P.: Particulate and dissolved aluminum and
605 titanium in the upper water column of the Atlantic Ocean, *Deep. Res. Part I Oceanogr. Res. Pap.*, 73, 127–139,
606 doi:10.1016/j.dsr.2012.12.002, 2013.

607 Dehairs, F., Jacquet, S., Savoye, N., Van Mooy, B. A. S., Buesseler, K. O., Bishop, J. K. B., Lamborg, C. H.,
608 Elskens, M., Baeyens, W., Boyd, P. W., Casciotti, K. L. and Monnin, C.: Barium in twilight zone suspended
609 matter as a potential proxy for particulate organic carbon remineralization: Results for the North Pacific, *Deep.*
610 *Res. Part II Top. Stud. Oceanogr.*, 55(14–15), 1673–1683, doi:10.1016/j.dsr2.2008.04.020, 2008.

611 Dutay, J. C., Tagliabue, A., Kriest, I. and van Hulten, M. M. P.: Modelling the role of marine particle on large
612 scale ^{231}Pa , ^{230}Th , Iron and Aluminium distributions, *Prog. Oceanogr.*, 133, 66–72,
613 doi:10.1016/j.pocean.2015.01.010, 2015.

614 Eittrheim, S., Thorndike, E. M. and Sullivan, L.: Turbidity distribution in the Atlantic Ocean, *Deep. Res. Oceanogr.*
615 *Abstr.*, 23(12), 1115–1127, doi:10.1016/0011-7471(76)90888-3, 1976.

616 Elderfield, H. and Schultz, A.: Mid-Ocean Ridge Hydrothermal Fluxes and the Chemical Composition of the
617 Ocean, *Annu. Rev. Earth Planet. Sci.*, 24(1), 191–224, doi:10.1146/annurev.earth.24.1.191, 1996.

618 Ellwood, M. J., Nodder, S. D., King, A. L., Hutchins, D. A., Wilhelm, S. W. and Boyd, P. W.: Pelagic iron cycling
619 during the subtropical spring bloom, east of New Zealand, *Mar. Chem.*, 160, 18–33,
620 doi:10.1016/j.marchem.2014.01.004, 2014.

621 Elrod, V. A., Berelson, W. M., Coale, K. H. and Johnson, K. S.: The flux of iron from continental shelf sediments:
622 A missing source for global budgets, *Geophys. Res. Lett.*, 31(12), 2–5, doi:10.1029/2004GL020216, 2004.

623 Fitzwater, S. E., Johnson, K. S., Gordon, R. M., Coale, K. H. and Smith, W. O.: Trace metal concentrations in
624 the Ross Sea and their relationship with nutrients and phytoplankton growth, *Deep. Res. Part II Top. Stud.*
625 *Oceanogr.*, 47(15–16), 3159–3179, doi:10.1016/S0967-0645(00)00063-1, 2000.

626 Fragoso, G. M., Poulton, A. J., Yashayaev, I. M., Head, E. J. H., Stinchcombe, M. C. and Purdie, D. A.:
627 Biogeographical patterns and environmental controls of phytoplankton communities from contrasting
628 hydrographical zones of the Labrador Sea, *Prog. Oceanogr.*, 141, 212–226, doi:10.1016/j.pocean.2015.12.007,
629 2016.

630 Frew, R. D., Hutchins, D. A., Nodder, S., Sanudo-Wilhelmy, S., Tovar-Sanchez, A., Leblanc, K., Hare, C. E. and
631 Boyd, P. W.: Particulate iron dynamics during FeCycle in subantarctic waters southeast of New Zealand, *Global*
632 *Biogeochem. Cycles*, 20(1), 1–15, doi:10.1029/2005GB002558, 2006.

633 García-Ibáñez, M. I., Pardo, P. C., Carracedo, L. I., Mercier, H., Lherminier, P., Ríos, A. F. and Pérez, F. F.:
634 Structure, transports and transformations of the water masses in the Atlantic Subpolar Gyre, *Prog. Oceanogr.*, 135,
635 18–36, doi:10.1016/j.pocean.2015.03.009, 2015.

636 Gardner, W. D., Tucholke, B. E., Richardson, M. J. and Biscaye, P. E.: Benthic storms, nepheloid layers, and
637 linkage with upper ocean dynamics in the western North Atlantic, *Mar. Geol.*, 385, 304–327,
638 doi:10.1016/j.margeo.2016.12.012, 2017.

639 Gardner, W. D., Richardson, M. J. and Mishonov, A. V.: Global assessment of benthic nepheloid layers and
640 linkage with upper ocean dynamics, *Earth Planet. Sci. Lett.*, 482, 126–134, doi:10.1016/j.epsl.2017.11.008, 2018.

641 Gerringa, L. J. A., Rijkenberg, M. J. A., Schoemann, V., Laan, P. and de Baar, H. J. W.: Organic complexation
642 of iron in the West Atlantic Ocean, *Mar. Chem.*, 177, 434–446, doi:10.1016/j.marchem.2015.04.007, 2015.

643 Hawkings, J. R., Wadham, J. L., Tranter, M., Raiswell, R., Benning, L. G., Statham, P. J., Tedstone, A., Nienow,
644 P., Lee, K. and Telling, J.: Ice sheets as a significant source of highly reactive nanoparticulate iron to the oceans,
645 *Nat. Commun.*, 5(May), 1–8, doi:10.1038/ncomms4929, 2014.

646 Hwang, J., Druffel, E. R. M. and Eglinton, T. I.: Widespread influence of resuspended sediments on oceanic
647 particulate organic carbon: Insights from radiocarbon and aluminum contents in sinking particles, *Global*
648 *Biogeochem. Cycles*, 24(4), 1–10, doi:10.1029/2010GB003802, 2010.

649 Jeandel, C. and Oelkers, E. H.: The influence of terrigenous particulate material dissolution on ocean chemistry
650 and global element cycles, *Chem. Geol.*, 395, 50–66, doi:10.1016/j.chemgeo.2014.12.001, 2015.

651 Jeandel, C., Peucker-Ehrenbrink, B., Jones, M. T., Pearce, C. R., Oelkers, E. H., Godderis, Y., Lacan, F., Aumont,
652 O. and Arsouze, T.: Ocean margins: The missing term in oceanic element budgets?, *Eos, Transactions American*
653 *Geophysical Union*, 92(26), 217–224, doi: 10.1029/2011EO260001, 2011.

654 Jickells, T. D., An, Z. S., Andersen, K. K., Baker, A. R., Bergametti, C., Brooks, N., Cao, J. J., Boyd, P. W., Duce,
655 R. A., Hunter, K. A., Kawahata, H., Kubilay, N., LaRoche, J., Liss, P. S., Mahowald, N., Prospero, J. M., Ridgwell,
656 A. J., Tegen, I. and Torres, R.: Global iron connections between desert dust, ocean biogeochemistry, and climate,
657 *Science (80-.)*, 308(5718), 67–71, doi:10.1126/science.1105959, 2005.

658 Jouanneau, J. M., Garcia, C., Oliveira, A., Rodrigues, A., Dias, J. A. and Weber, O.: Dispersal and deposition of
659 suspended sediment on the shelf off the Tagus and Sado estuaries, S.W. Portugal, *Prog. Oceanogr.*, 42(1–4), 233–
660 257, doi:10.1016/S0079-6611(98)00036-6, 1998.

661 Labatut, M., Lacan, F., Pradoux, C., Chmeleff, J., Radic, A., Murray, J. W., Poitrasson, F., Johansen, A. M., Thil,
662 F., Lacan, F., Pradoux, C., Chmeleff, J., Radic, A., Murray, J. W., Poitrasson, F., Johansen, A. M. and Thil, F.:
663 Iron sources and dissolved - particulate interactions in the seawater of the Western Equatorial Pacific, iron isotope
664 perspectives., *Global Biogeochem Cycles*, 1044–1065, doi:10.1002/2014GB004928, 2014.

665 Lam, P. J. and Bishop, J. K. B.: The continental margin is a key source of iron to the HNLC North Pacific Ocean,
666 *Geophys. Res. Lett.*, 35(7), 1–5, doi:10.1029/2008GL033294, 2008.

667 Lam, P. J., Ohnemus, D. C. and Marcus, M. A.: The speciation of marine particulate iron adjacent to active and
668 passive continental margins, *Geochim. Cosmochim. Acta*, 80, 108–124, doi:10.1016/j.gca.2011.11.044, 2012.

669 Lam, P. J., Ohnemus, D. C. and Auro, M. E.: Size-fractionated major particle composition and concentrations
670 from the US GEOTRACES North Atlantic Zonal Transect, *Deep. Res. Part II Top. Stud. Oceanogr.*, 116, 303–
671 320, doi:10.1016/j.dsr2.2014.11.020, 2015.

672 Lam, P. J., Lee, J. M., Heller, M. I., Mehic, S., Xiang, Y. and Bates, N. R.: Size-fractionated distributions of
673 suspended particle concentration and major phase composition from the U.S. GEOTRACES Eastern Pacific Zonal
674 Transect (GP16), *Mar. Chem.*, (April), 0–1, doi:10.1016/j.marchem.2017.08.013, 2017.

675 Lannuzel, D., Bowie, A. R., van der Merwe, P. C., Townsend, A. T. and Schoemann, V.: Distribution of dissolved
676 and particulate metals in Antarctic sea ice, *Mar. Chem.*, 124(1–4), 134–146, doi:10.1016/j.marchem.2011.01.004,
677 2011.

678 Lannuzel, D., Van der Merwe, P. C., Townsend, A. T. and Bowie, A. R.: Size fractionation of iron, manganese
679 and aluminium in Antarctic fast ice reveals a lithogenic origin and low iron solubility, *Mar. Chem.*, 161, 47–56,
680 doi:10.1016/j.marchem.2014.02.006, 2014.

681 Lee, J. M., Heller, M. I. and Lam, P. J.: Size distribution of particulate trace elements in the U.S. GEOTRACES
682 Eastern Pacific Zonal Transect (GP16), *Mar. Chem.*, 201(September 2017), 108–123,
683 doi:10.1016/j.marchem.2017.09.006, 2017.

684 Lemaitre, N., planquette, H., Planchon, F., Sarthou, G., Jacquet, S., Garcia-Ibanez, M. I., Gourain, A., Cheize, M.,
685 Monin, L., Andre, L., Laha, P., Terryn, H., and Dehairs, F.: Particulate barium tracing significant mesopelagic
686 carbon remineralisation in the North Atlantic, *Biogeosciences*, doi:10.5194/bg-15-2289-2018, 2018a.

687 Lemaitre, N., Planchon, F., Planquette, H., Dehairs, F., Fonseca-Batista, D., Roukaerts, A., Deman, F., Tang, Y.,
688 Mariez, C., and Sarthou G.: High variability of export fluxes along the North Atlantic GEOTRACES section
689 GA01: Particulate organic carbon export deduced from the ²³⁴Th method, *Biogeosciences*, doi:10.5194/bg-2018-
690 190, 2018b.

691 Le Roy, E., Sanial, V., Charette, M.A., Van Beek, P., Lacan, F., Jacquet, S.H., Henderson, P.B., Souhaut, M.,
692 García-Ibáñez, M.I., Jeandel, C. and Pérez, F.: The ²²⁶Ra-Ba relationship in the North Atlantic during
693 GEOTRACES-GA01, *Biogeosciences*, doi:10.5194/bg-2017-478, 2017.

694 Marsay, C. M., Lam, P. J., Heller, M. I., Lee, J. M. and John, S. G.: Distribution and isotopic signature of ligand-
695 leachable particulate iron along the GEOTRACES GP16 East Pacific Zonal Transect, *Mar. Chem.*, (November
696 2016), 1–14, doi:10.1016/j.marchem.2017.07.003, 2017.

697 Martin, J. H., Fitzwater, S. E., Michael Gordon, R., Hunter, C. N. and Tanner, S. J.: Iron, primary production and
698 carbon-nitrogen flux studies during the JGOFS North Atlantic bloom experiment, *Deep. Res. Part II*, 40(1–2),
699 115–134, doi:10.1016/0967-0645(93)90009-C, 1993.

700 McCave, I. N. and Hall, I. R.: Turbidity of waters over the Northwest Iberian continental margin, *Prog. Oceanogr.*,
701 52(2–4), 299–313, doi:10.1016/S0079-6611(02)00012-5, 2002.

702 Menzel Barraqueta, J.L., Schlosser, C., Planquette, H., Gourain, A., Cheize, M., Boutorh, J., Shelley, R., Pereira
703 Contreira, L., Gledhill, M., Hopwood, M.J. and Lherminier, P.: Aluminium in the North Atlantic Ocean and the

704 Labrador Sea (GEOTRACES GA01 section): roles of continental inputs and biogenic particle removal.
705 *Biogeosciences*, 1-28, doi: 10.5194/bg-2018-39, 2018.

706 Milne, A., Schlosser, C., Wake, B. D., Achterberg, E. P., Chance, R., Baker, A. R., Forryan, A. and Lohan, M.
707 C.: Particulate phases are key in controlling dissolved iron concentrations in the (sub)tropical North Atlantic,
708 *Geophys. Res. Lett.*, 44(5), 2377–2387, doi:10.1002/2016GL072314, 2017.

709 Nuester, J., Shema, S., Vermont, A., Fields, D. M. and Twining, B. S.: The regeneration of highly bioavailable
710 iron by meso- and microzooplankton, *Limnol Oceanogr.*, 59(4), 1399–1409, doi:10.4319/lo.2014.59.4.1399, 2014.

711 Oelkers, E. H., Jones, M. T., Pearce, C. R., Jeandel, C., Eiriksdottir, E. S. and Gislason, S. R.: Riverine particulate
712 material dissolution in seawater and its implications for the global cycles of the elements, *Geosci.*, 344(11–12),
713 646–651, doi:10.1016/j.crte.2012.08.005, 2012.

714 Ohnemus, D. C. and Lam, P. J.: Cycling of lithogenic marine particles in the US GEOTRACES North Atlantic
715 transect, *Deep. Res. Part II Top. Stud. Oceanogr.*, 116, 283–302, doi:10.1016/j.dsr2.2014.11.019, 2015.

716 Peers, G. and Price, N. M.: A role for manganese in superoxide dismutases and growth of iron-deficient diatoms,
717 *Limnol. Oceanogr.*, 49(5), 1774–1783, doi:10.4319/lo.2004.49.5.1774, 2004.

718 Planquette, H. and Sherrell, R. M.: Sampling for particulate trace element determination using water sampling
719 bottles: Methodology and comparison to in situ pumps, *Limnol. Oceanogr. Methods*, 10(5), 367–388,
720 doi:10.4319/lom.2012.10.367, 2012.

721 Planquette, H., Fones, G. R., Statham, P. J. and Morris, P. J.: Origin of iron and aluminium in large particles (>
722 53 μm) in the Crozet region, Southern Ocean, *Mar. Chem.*, 115(1–2), 31–42, doi:10.1016/j.marchem.2009.06.002,
723 2009.

724 Planquette, H., Sanders, R. R., Statham, P. J., Morris, P. J. and Fones, G. R.: Fluxes of particulate iron from the
725 upper ocean around the Crozet Islands: A naturally iron-fertilized environment in the Southern Ocean, *Global*
726 *Biogeochem. Cycles*, 25(2), doi:10.1029/2010GB003789, 2011.

727 Planquette, H., Sherrell, R. M., Stammerjohn, S. and Field, M. P.: Particulate iron delivery to the water column
728 of the Amundsen Sea, Antarctica, *Mar. Chem.*, 153, 15–30, doi:10.1016/j.marchem.2013.04.006, 2013.

729 Radic, A., Lacan, F. and Murray, J. W.: Iron isotopes in the seawater of the equatorial Pacific Ocean: New
730 constraints for the oceanic iron cycle, *Earth Planet. Sci. Lett.*, 306(1–2), 1–10, doi:10.1016/j.epsl.2011.03.015,
731 2011.

732 Raiswell, R., Benning, L. G., Tranter, M. and Tulaczyk, S.: Bioavailable iron in the Southern Ocean: The
733 significance of the iceberg conveyor belt, *Geochem. Trans.*, 9(1), 7, doi:10.1186/1467-4866-9-7, 2008.

734 Rijkenberg, M. J. A., Middag, R., Laan, P., Gerringa, L. J. A., Van Aken, H. M., Schoemann, V., De Jong, J. T.
735 M. and De Baar, H. J. W.: The distribution of dissolved iron in the West Atlantic Ocean, PLoS One, 9(6), 1–14,
736 doi:10.1371/journal.pone.0101323, 2014.

737 Sanders, R., Henson, S. A., Koski, M., De La Rocha, C. L., Painter, S. C., Poulton, A. J., Riley, J., Salihoglu, B.,
738 Visser, A., Yool, A., Bellerby, R. and Martin, A. P.: The Biological Carbon Pump in the North Atlantic, Prog.
739 Oceanogr., 129(PB), 200–218, doi:10.1016/j.pocean.2014.05.005, 2014.

740 Sarthou, G., Lherminier, and the GEOVIDE team: Introduction to the French GEOTRACES North Atlantic
741 Transect (GA01): GEOVIDE cruise, Biogeosciences, 15, 7097–7109, <https://doi.org/10.5194/bg-15-7097-2018>,
742 2018.

743 Sarthou, G., Vincent, D., Christaki, U., Obernosterer, I., Timmermans, K. R. and Brussaard, C. P. D.: The fate of
744 biogenic iron during a phytoplankton bloom induced by natural fertilisation: Impact of copepod grazing, Deep.
745 Res. Part II Top. Stud. Oceanogr., 55(5–7), 734–751, doi:10.1016/j.dsr2.2007.12.033, 2008.

746 Schlosser, C., Schmidt, K., Aquilina, A., Homoky, W. B., Castrillejo, M., Mills, R. A., Patey, M. D., Fielding, S.,
747 Atkinson, A. and Achterberg, E. P.: Mechanisms of dissolved and labile particulate iron supply to shelf waters
748 and phytoplankton blooms off South Georgia, Southern Ocean, Biogeosciences Discuss., 0049(July), 1–49,
749 doi:10.5194/bg-2017-299, 2017.

750 Shelley, R. U., Landing, W. M., Ussher, S. J., Planquett, H. and Sarthou, G.: Characterisation of aerosol
751 provenance from the fractional solubility of Fe (Al, Ti, Mn, Co, Ni, Cu, Zn, Cd and Pb) in North Atlantic aerosols
752 (GEOTRACES GA01 and GA03), Biogeosciences, submitted(November), 1–31, doi:10.5194/bg-2017-415,
753 2017.

754 Shelley, R. U., Landing, W. M., Ussher, S. J., Planquette, H. and Sarthou, G.: Regional trends in the fractional
755 solubility of Fe and other metals from North Atlantic aerosols (GEOTRACES cruises GA01 and GA03) following
756 a two-stage leach, Biogeosciences, 15(1), 2271–2288, doi:10.5194/bg-15-2271-2018, 2018.

757 Sherrell, R. M., Field, P. M. and Gao, Y.: Temporal variability of suspended mass and composition in the
758 Northeast Pacific water column: Relationships to sinking flux and lateral advection, Deep. Res. Part II Top. Stud.
759 Oceanogr., 45(4–5), 733–761, doi:10.1016/S0967-0645(97)00100-8, 1998.

760 Spinrad, R. W., Zaneveld, J. R. and Kitchen, J.C.: A Study of the Optical Characteristics of the Suspended Particles
761 Benthic Nepheloid Layer of the Scotian Rise, J. Geophys. Res., 88, 7641–7645, doi:10.1029/1983JC00303C, 1983.

762 Statham, P. J., Skidmore, M. and Tranter, M.: Inputs of glacially derived dissolved and colloidal iron to the coastal
763 ocean and implications for primary productivity, Global Biogeochem. Cycles, 22(3), 1–11,
764 doi:10.1029/2007GB003106, 2008.

765 Straneo, F., Pickart, R. S. and Lavender, K.: Spreading of Labrador sea water: An advective-diffusive study based
766 on Lagrangian data, *Deep. Res. Part I Oceanogr. Res. Pap.*, 50(6), 701–719, doi:10.1016/S0967-0637(03)00057-
767 8, 2003.

768 Sunda, W. G. and Huntsman, S. A.: Effect of Competitive Interactions Between Manganese and Copper on
769 Cellular Manganese and Growth in Estuarine and Oceanic Species of the Diatom *Thalassiosira*, *Limnol.*
770 *Oceanogr.*, 28(5), 924–934, doi:10.4319/lo.1983.28.5.0924, 1983.

771 Tagliabue, A., Bopp, L., Dutay, J. C., Bowie, A. R., Chever, F., Jean-Baptiste, P., Bucciarelli, E., Lannuzel, D.,
772 Remenyi, T., Sarthou, G., Aumont, O., Gehlen, M. and Jeandel, C.: Hydrothermal contribution to the oceanic
773 dissolved iron inventory, *Nat. Geosci.*, 3(4), 252–256, doi:10.1038/ngeo818, 2010.

774 Tagliabue, A., Bowie, A. R., Boyd, P. W., Buck, K. N., Johnson, K. S. and Saito, M. A.: The integral role of iron
775 in ocean biogeochemistry, *Nature*, 543(7643), 51–59, doi:10.1038/nature21058, 2017.

776 Taylor, S. and McLennan, S.: The geochemical evolution of the continental crust, *Rev. Geophys.*, 33(2), 241–
777 265, doi:10.1029/95RG00262, 1995.

778 Tebo, B. M. and Emerson, S. R.: Effect of Oxygen Tension Manganese (II) Concentration and Temperature on
779 the Microbially Catalyzed Manganese-Ii Oxidation Rate in a Marine Fjord, *Appl. Environ. Microbiol.*, 50(5),
780 1268–1273, 1985.

781 Tebo, B. M., Nealson, K. H., Emerson, S. and Jacobs, L.: Microbial mediation of Mn(II) and Co(II) precipitation
782 at the o₂/H₂S interfaces in two anoxic fjords, 29(6), 1247–1258, 1984.

783 Tonnard, M., Planquette, H., Bowie, A. R., van der Merwe, P., Gallinari, M., Desprez de Gésincourt, F., Germain,
784 Y., Gourain, A., Benetti, M., Reverdin, G., Tréguer, P., Boutorh, J., Cheize, M., Menzel Barraqueta, J., Pereira-
785 Contreira, L., Shelley, R., Lherminier, P., and Sarthou, G.: Dissolved iron in the North Atlantic Ocean and
786 Labrador Sea along the GEOVIDE section (GEOTRACES section GA01), *Biogeosciences Discuss.*,
787 <https://doi.org/10.5194/bg-2018-147>, 2018

788 Trefry, J. H., Trocine, R. P., Klinkhammer, G. P. and Rona, P. A.: Iron and copper enrichment of suspended
789 particles in dispersed hydrothermal plumes along the mid-Atlantic Ridge, *Geophys. Res. Lett.*, 12(8), 506–509,
790 doi:10.1029/GL012i008p00506, 1985.

791 Ussher, S. J., Achterberg, E. P. and Worsfold, P. J.: Marine biogeochemistry of iron, *Environ. Chem.*, 1(2), 67–
792 80, doi:10.1071/EN04053, 2004.

793 Ussher, S. J., Worsfold, P. J., Achterberg, E. P., Laës, A., Blain, S., Laan, P., de Baar, H. J. W.: Distribution and
794 redox speciation of dissolved iron on the European continental margin, *Limnol. Oceanogr.*, 52(6), 2530–2539,
795 doi:10.4319/lo.2007.52.6.2530, 2007.

796 Van der Merwe, P., Lannuzel, D., Bowie, A. R., Mancuso Nichols, C. A. and Meiners, K. M.: Iron fractionation
797 in pack and fast ice in East Antarctica: Temporal decoupling between the release of dissolved and particulate iron

798 during spring melt, *Deep. Res. Part II Top. Stud. Oceanogr.*, 58(9–10), 1222–1236,
799 doi:10.1016/j.dsr2.2010.10.036, 2011a.

800 Van Der Merwe, P., Lannuzel, D., Bowie, A. R. and Meiners, K. M.: High temporal resolution observations of
801 spring fast ice melt and seawater iron enrichment in East Antarctica, *J. Geophys. Res. Biogeosciences*, 116(3), 1–
802 18, doi:10.1029/2010JG001628, 2011b.

803 Weinstein, S. E. and Moran, S. B.: Distribution of size-fractionated particulate trace metals collected by bottles
804 and in-situ pumps in the Gulf of Maine-Scotian Shelf and Labrador Sea, *Mar. Chem.*, 87(3–4), 121–135,
805 doi:10.1016/j.marchem.2004.02.004, 2004.

806 Yashayaev, I.: Hydrographic changes in the Labrador Sea, 1960-2005, *Prog. Oceanogr.*, 73(3–4), 242–276,
807 doi:10.1016/j.pocean.2007.04.015, 2007.

808 Yashayaev, I. and Loder, J. W.: Enhanced production of Labrador Sea Water in 2008, *Geophys. Res. Lett.*, 36(1),
809 doi:10.1029/2008GL036162, 2009.

810 Zunino, P., Lherminier, P., Mercier, H., Daniault, N., García-Ibáñez, M. I., and Pérez, F. F.: The GEOVIDE
811 cruise in May–June 2014 reveals an intense Meridional Overturning Circulation over a cold and fresh subpolar
812 North Atlantic. *Biogeosciences*, 14(23), 5323, 2017.

813

814

815

816

817

818

819

820

821

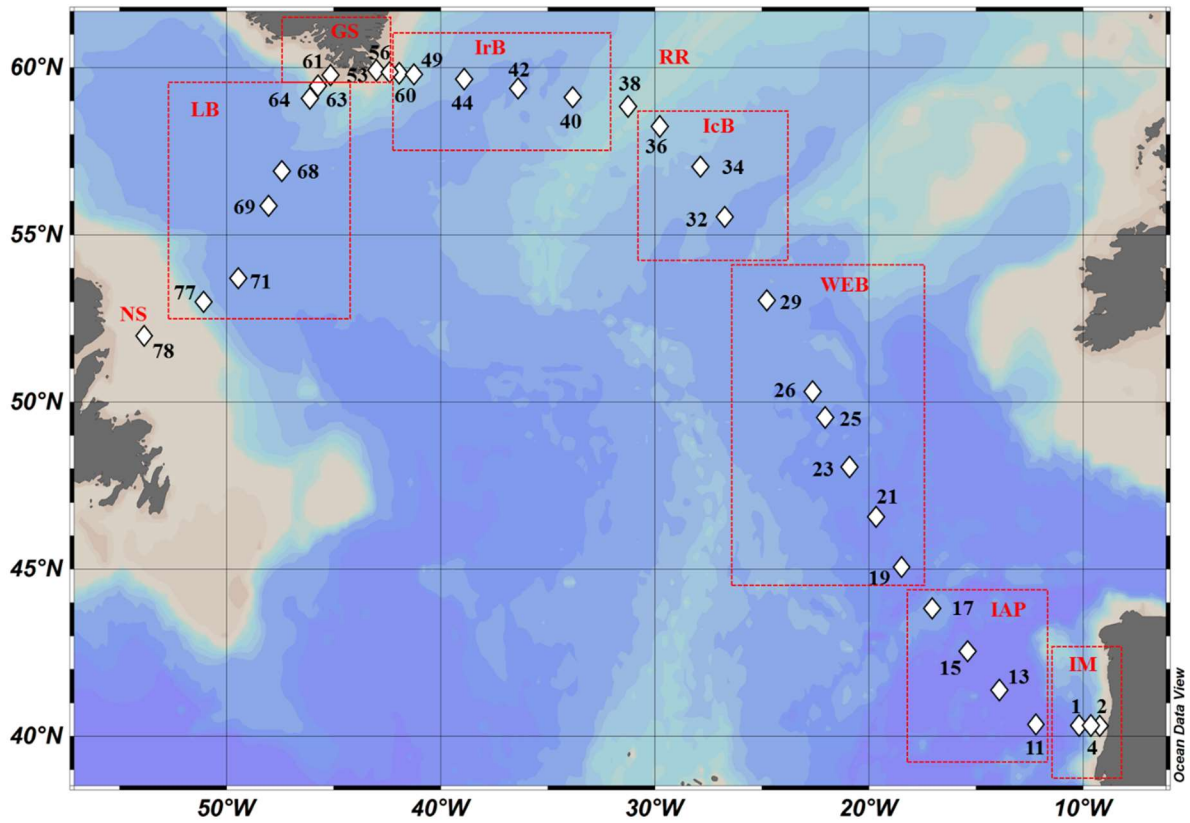
822

823

824

825

826 **Figure 1: Map of stations where suspended particle samples were collected with GO-FLO bottles during the GEOVIDE**
827 **cruise (GA01). Biogeochemical provinces are indicated by red squares, IM: Iberian Margin, IAP: Iberian Abyssal**
828 **Plain, WEB: Western European Basin, IcB: Iceland Basin, RR: Reykjanes Ridge, IrB: Irminger Basin, GS: Greenland**
829 **Shelf, LB: Labrador Basin, NS: Newfoundland Shelf. This figure was generated by Ocean Data View (Schlitzer, R.,**
830 **Ocean Data View, odv.awi.de, 2017).**



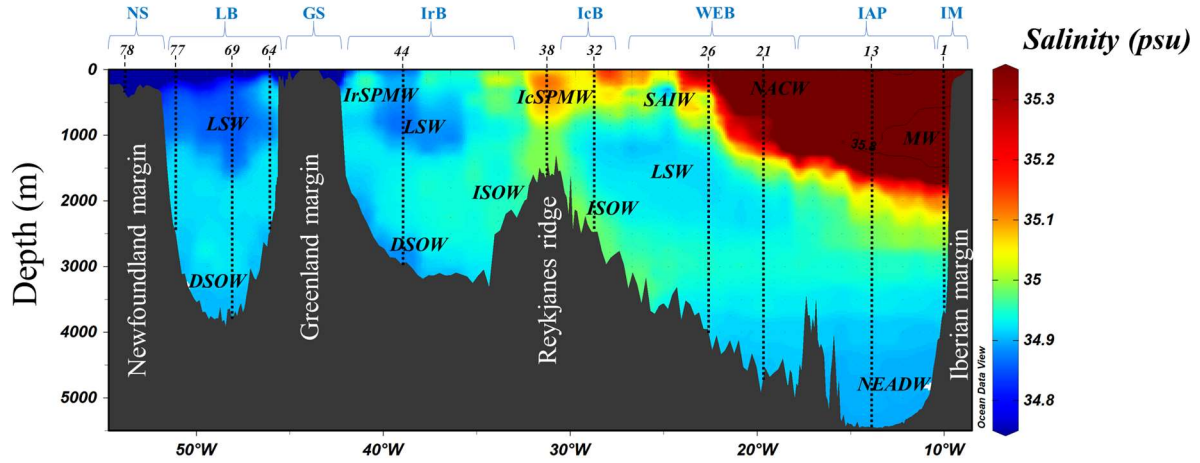
831
 832
 833
 834
 835
 836
 837
 838
 839
 840
 841
 842
 843
 844
 845
 846

847 **Figure 2: Salinity section during the GEOVIDE cruise. Water masses are indicated in black, MW: Mediterranean**
 848 **Water; NACW: North Atlantic Central Water; NEADW: North East Atlantic Deep Water; LSW: Labrador Sea**
 849 **Water; DSOW: Denmark Strait Overflow Water; ISOW: Iceland-Scotland Overflow Water; SAIW: Sub-Arctic**
 850 **Intermediate Water; IcSPMW: Iceland Sub-Polar Mode Water; IrSPMW: Irminger Sub-Polar Mode Water. Station**
 851 **locations are indicated by the numbers. Biogeochemical provinces are indicated in blue font above station numbers.**

852 Contour of salinity = 35.8psu have been applied to identify the Mediterranean Water. This figure was generated by
 853 Ocean Data View (Schlitzer, R., Ocean Data View, odv.awi.de, 2017).

854

855



856

857

858

859

860

861

862

863

864

865

866

867

868

869

870

871

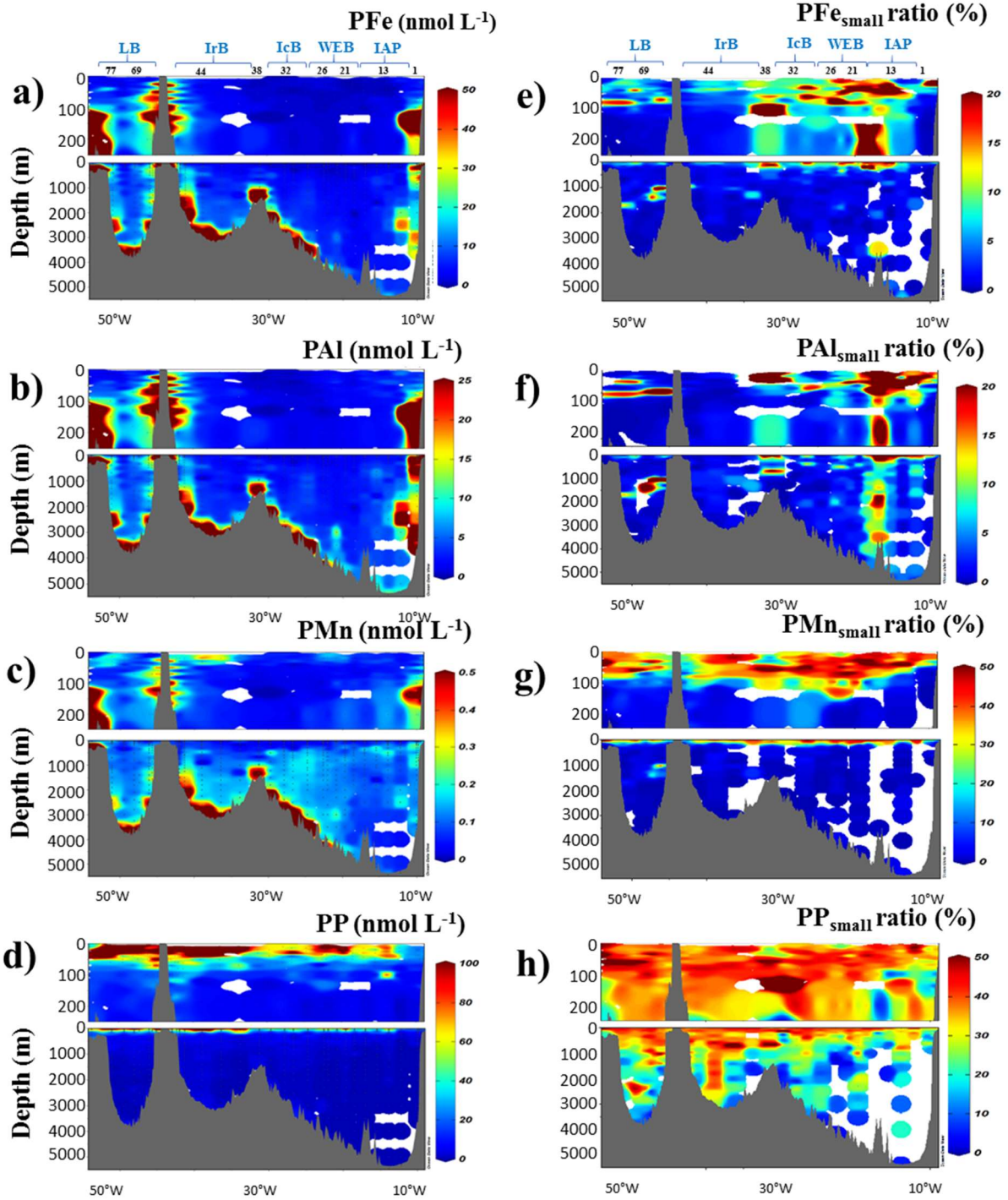
872

873

874

875

876 Figure 3: Left) Distribution of total particulate iron (a, PFe), aluminium (b, PAI), manganese (c, PMn) and phosphorus
 877 (d, PP) concentrations (in nmol L^{-1}) along the GEOVIDE section. Right) Contribution of small size fraction (0.45-5 μm)
 878 expressed as percentage (%) of the total concentration of PFe (e), PAI (f), PMn (g) and PP (h). Station IDs and
 879 biogeochemical region are indicated on top of section a. This figure was generated by Ocean Data View (Schlitzer, R.,
 880 Ocean Data View, odv.awi.de, 2017).

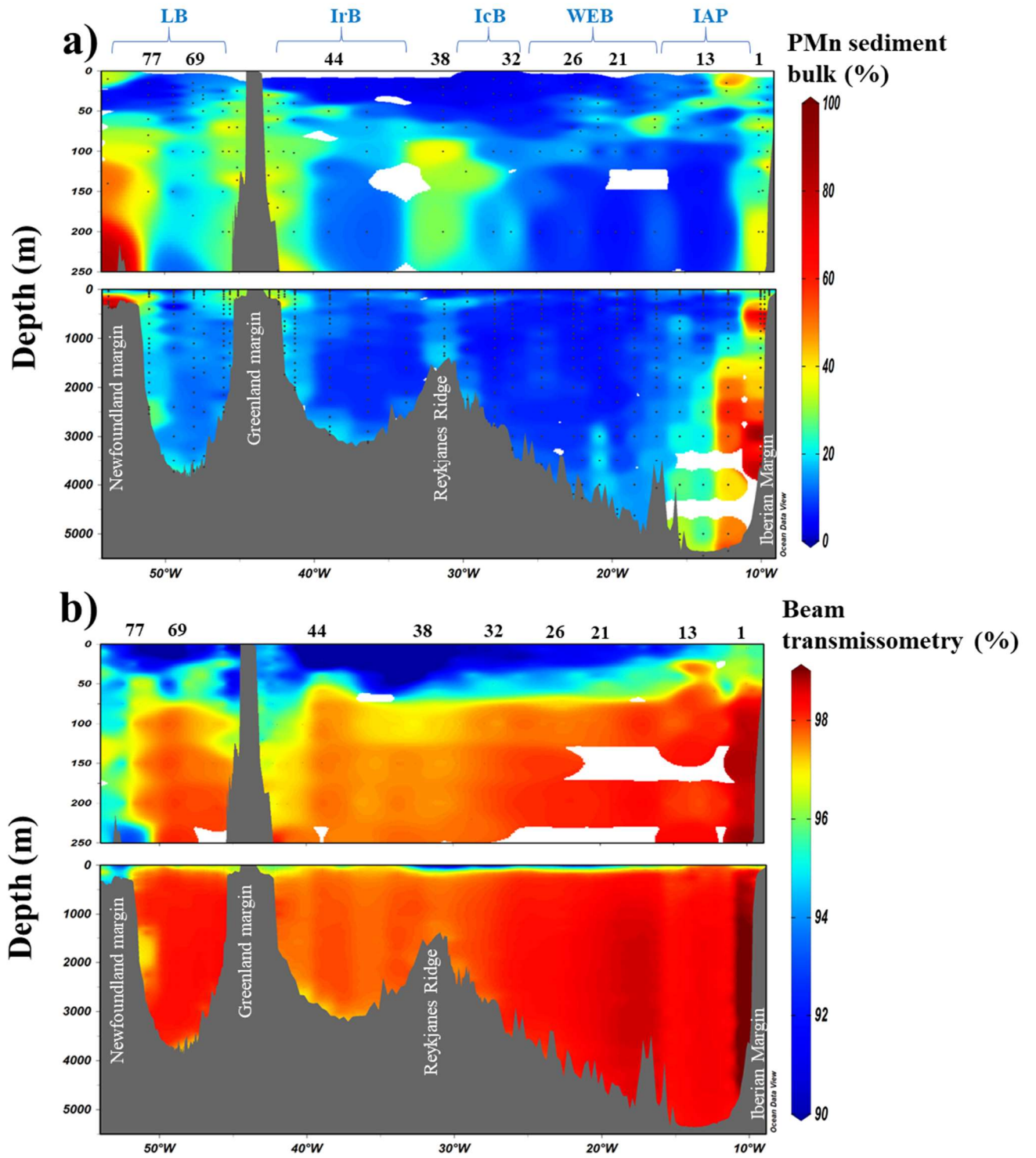


881

882

883

884 Figure 4: Section of derived contribution of sedimentary inputs manganese bulk sediment proxy (a) and
 885 transmissometry (b) along the GA01 section. Station IDs and biogeochemical region are indicated above the section (a).
 886 This figure was generated by Ocean Data View (Schlitzer, R., Ocean Data View, odv.awi.de, 2017).



887

888

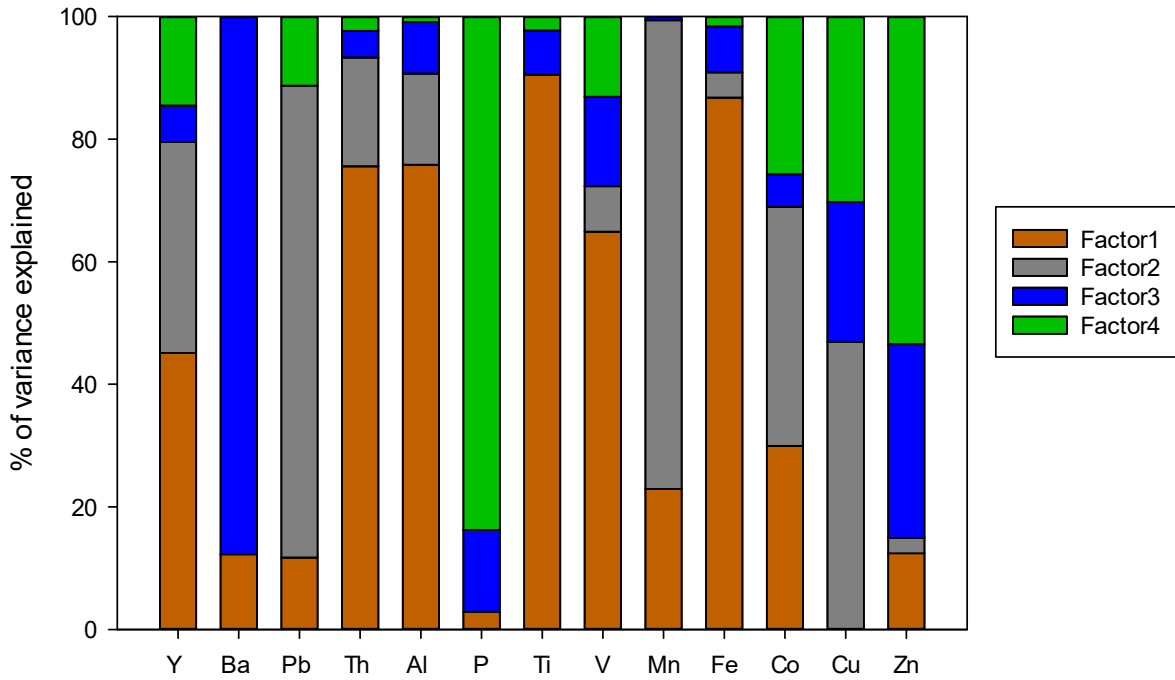
889

890

891

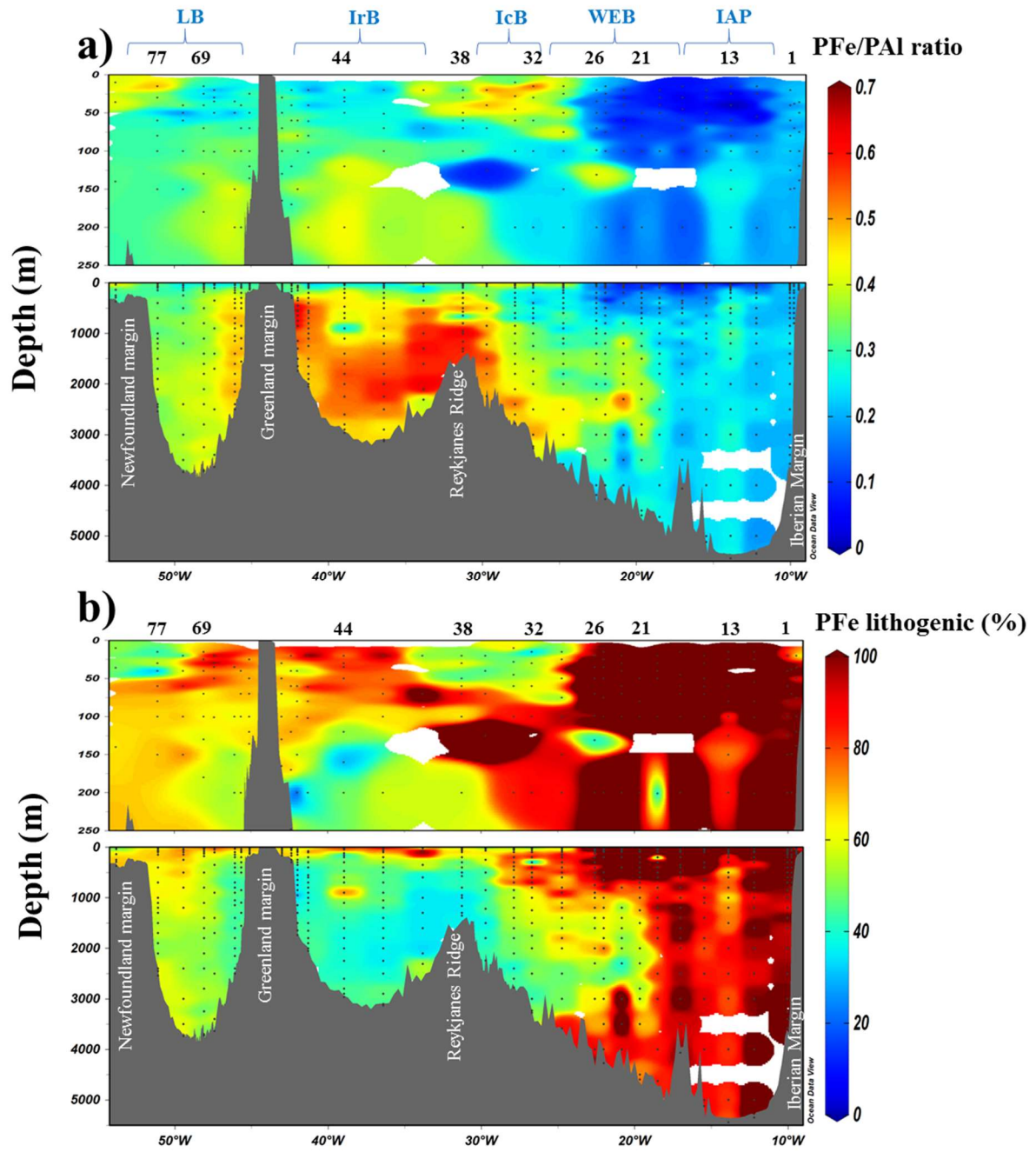
892

893 Figure 5: Factor fingerprint of the positive matrix factorisation. The four factors are represented in a stacked bar chart
 894 of the percentage of variance explained per element.



895
 896
 897
 898
 899
 900
 901
 902
 903
 904
 905
 906
 907
 908
 909
 910
 911
 912
 913

914 Figure 6: a) Section of the PFe to PAI molar ratio (mol mol^{-1}); (b) contribution of $\text{PFe}_{\text{litho}}(\%)$ based on Eq. (1). Station
 915 IDs and biogeochemical provinces are indicated above each section. This figure was generated by Ocean Data View
 916 (Schlitzer, R., Ocean Data View, odv.awi.de, 2017).



917

918

919

920

921

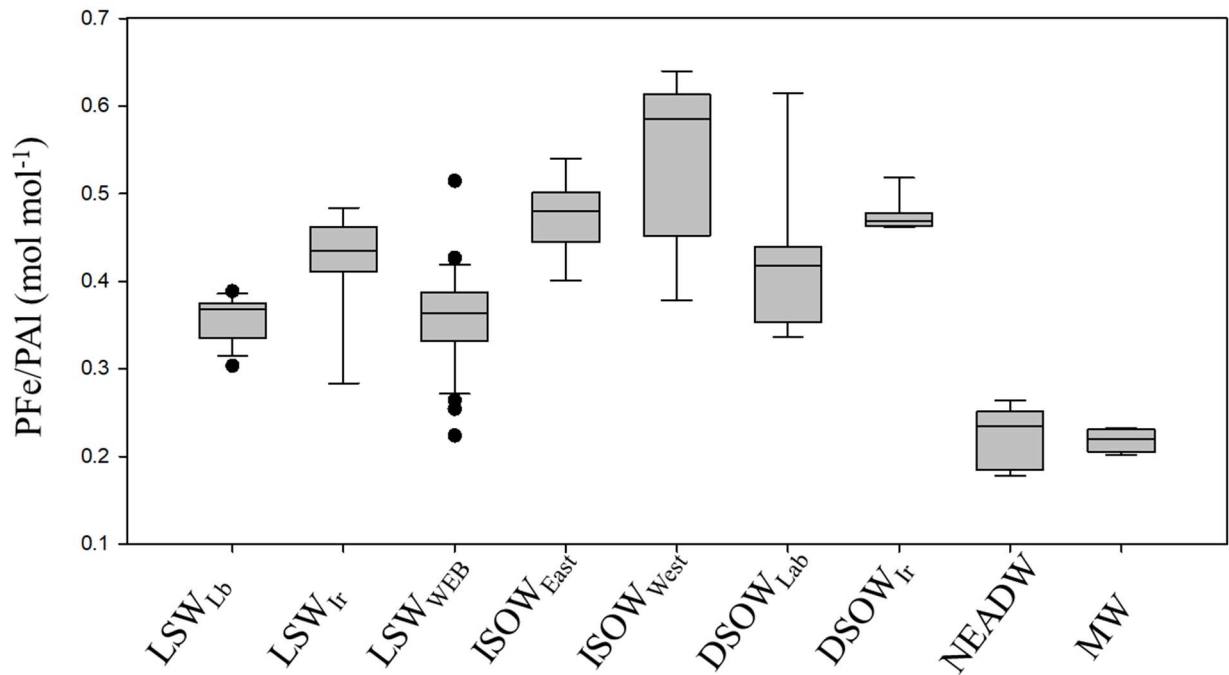
922

923

924 **Figure 7: Whisker diagram of PFe/PAI molar ratio (mol mol⁻¹) in the different water masses sampled along the GA01**
 925 **line. Median values for the water masses were as follows: LSW_{lb}= 0.37; LSW_{lr}=0.44; LSW_{WEB}=0.36; ISOW_{east}=0.48;**
 926 **ISOW_{west}=0.58; DSOW_{lab}=0.42; DSOW_{lr}=0.47; NEADW=0.23; MW=0.22 mol mol⁻¹. Based on their salinity and**
 927 **potential temperature signatures (García-Ibáñez et al., 2015; Figure 2), we applied a Kruskal-Wallis test on molar**
 928 **PFe/PAI ratios of nine water masses (Figure 7) in order to test the presence of significant differences. Water masses for**
 929 **which we had less than 5 data points for PFe/PAI were excluded from this test. As the differences in the median values**
 930 **among the treatment groups were greater than would be expected by chance; the difference in PFe/PAI between water**
 931 **masses is statistically significant (P = <0.001).**

932

933



934

935

936

937

938

939

940

941

942

943

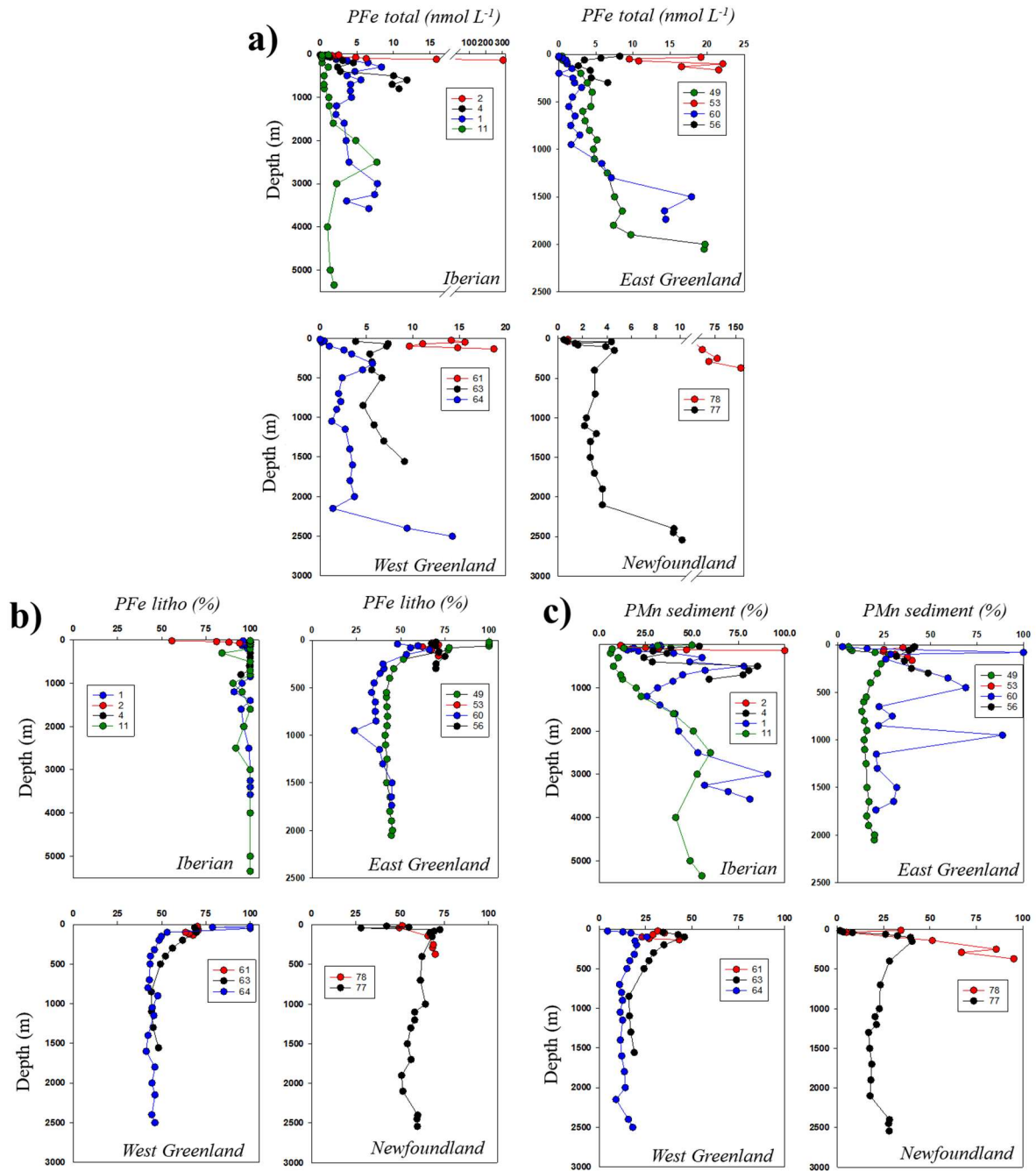
944

945

946

947

948 **Figure 8:** Vertical profiles of PFe (nmol L⁻¹, a), lithogenic proportion of particulate iron (PFe_{litho}, %, b) and sedimentary
 949 proportion of particulate manganese (PMn sediment, %, c) at the Iberian, East-West Greenland and Newfoundland
 950 margins.



951

952

953

954

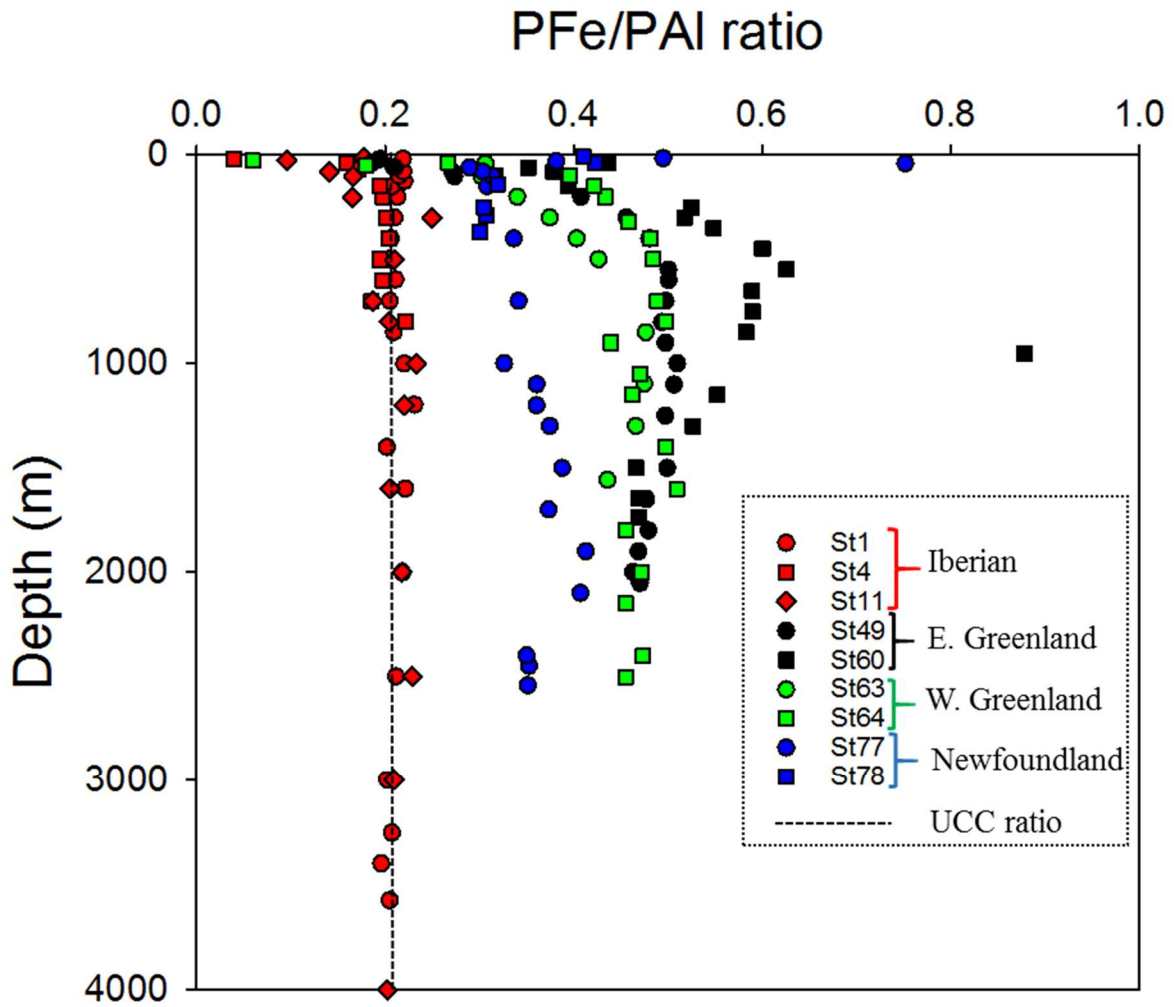
955

956

957

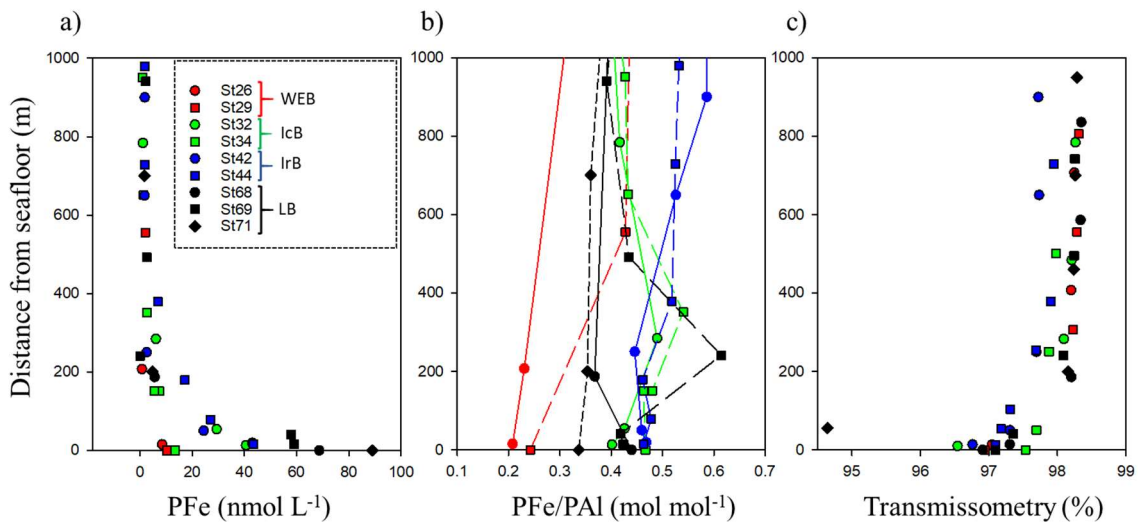
958
959

Figure 9: Scatter of the PFe/PAI ratio at the Iberian (red dots), East Greenland (black dots), West Greenland (green dots) and Newfoundland margins (blue dots). Dashed line indicate the UCC ratio (Taylor and McLennan, 1995).



960
961
962
963
964
965
966
967
968
969
970

971 **Figure 10: PFe total (a); PFe/PAI ratio (b) and beam transmissometry (%) as a function of depth above the seafloor**
 972 **(m) at selected stations where a decrease in transmissometry was recorded.**



973

974

975

976

977

978

979

980

981

982

983

984

985

986

987

988

		Fe	Al	P	Mn
Blank (nmol L ⁻¹)	5µm filter	0.072	0.100	0.511	0.003
	0.45µm filter	0.132	0.164	1.454	0.005
Limit of detection (nmol L ⁻¹)	5µm filter	0.011	0.030	0.365	0.001
	0.45µm filter	0.026	0.046	1.190	0.001
Recovery CRM (%)	BCR-414 (n=10)	88 ± 7			94 ± 7
	MESS-4 (n=5)	98 ± 14	97 ± 14	80 ± 30	110 ± 18
	PACS-3 (n=8)	101 ± 9	99 ± 14	91 ± 34	112 ± 11

989

990 **Table 1: Blank and limit of detection (nmol L⁻¹) of the two filters and Certified reference material (CRM)**
991 **recoveries during GEOVIDE suspended particle digestion.**

992

993

Author	Year	Fraction	Location	Depth range	PFe	PAI	PMn	PP
This study		>0.45µm	N. Atlantic (>40°N)	All	bdl-304	bdl-1544	bdl-3.5	bdl-402
Barrett et al.	2012	0.4µm	N. Atlantic (25-60°N)	Upper 1000m	0.29-1.71	0.2-19.7		
Dammshäuser et al.	2013	>0.2 µm	Eastern tropical N.A.	0-200		0.59-17.7		
Dammshäuser et al.	2013	>0.2 µm	Meridional Atlantic	0-200		0.35-16.1		
Lam et al.	2012	1–51 µm	Eastern tropical N.A.	0-600	ND-12			
Lannuzel et al.	2011	>0.2 µm	East Antarctic	Surface		0.02-10.67	0.01-0.14	
Lannuzel et al.	2014	>0.2 µm	East Antarctic	Fast ice	43-10385	121-31372	1-307	
Lee et al.	2017	>0.8 µm	Eastern tropical S.Pacific	All	bdl-159	bdl-162	bdl-8.7	bdl-983
Marsay et al.	2017	>0.4 µm	Ross Sea	All	0.68-57.3	ND-185	ND-1.4	5.4-404
Milne et al.	2017	>0.45µm	Sub-tropical N.A.	All	ND-140	ND-800		
Ohnemus et al.	2015	0.8–51 µm	N. Atlantic	All	0-938	0-3600		
Planquette et al.	2009	>53 µm	Southern Ocean	30-340	0.15–13.2	0.11–25.5		
Schlosser et al.	2017	>1 µm	South Georgia Shelf	All	0.87-267	0.6-195	0.01-3.85	
Sherrell et al.	1998	1-53µm	Northeast Pacific	0-3557		0.0-54.2		
Weinstein et al.	2004	>53 µm	Labrador Sea	0-250	0.1-1.2	0.1-1.5		
Weinstein et al.	2004	0.4– 10µm	Labrador Sea	0-250	2.5	3.6	0.05	
Weinstein et al.	2004	>0.4 µm	Gulf of Maine	0-300	34.8	109		

994

995 **Table 2: Concentration (in nmol L⁻¹) of trace elements (PFe, PAI, PMn and PP) in suspended particles collected in**
996 **diverse regions of the world's ocean. Bdl: below detection limit, ND: non-determined.**

997

998

999